

Dr. Florent Dominé  
Editor  
The Cryosphere

Davos, 10 March 2015

Benjamin Reuter  
WSL Institute for Snow and Avalanche Research SLF  
phone +41 81 417 0347, fax +41 81 417 0110  
reuter@slf.ch



**Submission of revised manuscript**

Dear Dr. Dominé,

we addressed all reviewers' questions and highlighted the changes in the manuscript.

We hope that the paper is acceptable for publication in The Cryosphere.

Sincerely,

Benjamin Reuter

(on behalf of all co-authors)

## Reply to Referee #1 (E.A. Podolskiy) RC C2912

I enjoyed reading this well-written and carefully prepared manuscript proposing an objective instability assessment technique, which is certainly addressing a problem at the core of snow avalanche forecasting.

The authors analyze tens of Snow-Micro-Penetrator (SMP) and Propagation Saw Tests (PST) against finite element (FE) predictions supported by previous analytical solutions in order to justify the proposed methodology, which is making an important step out of observer-dependent instability evaluation.

To me, clearly presented rationale, methods and results, supporting the developed approach, seem convincing and valuable for a wide community of snow avalanche professionals and snow scientists. Below I am listing only several minor remarks and points requiring, in my opinion, some more details or explanation.

### Abstract

Since the failure initiation criterion is a function of additional stress due to skier loading, this should be mentioned in the Abstract. E.g., L18: “. . . method for estimating snow instability {under skier loading}.” Doing so in the title is indeed your own decision.

*We agree that the mass of a skier is considered for the failure initiation criterion. However, the crack propagation is not linked to any kind of external loading. As we present two independent criteria, we do not prefer to introduce this limitation in the Abstract.*

p. 5827, L15

Provide a reference reporting such field observations.

*We inserted a reference to Perla (1977) in line 35 of the revised manuscript.*

p. 5827-5829

Somewhere in your review I advise you to mention a work by McClung (2009), which is strongly related to the domain of your paper.

*We now refer to the work by McClung (2009) as suggested (lines 76-77).*

p. 5829, L29

“force-distancesignal” - missing space

*Changed as suggested (line 88).*

p. 5833, L1-3

Here you describe derivation of the penetration depth and I could not follow which one do you mean. For example, in Fig. 3 the x-axis shows Depth, so that Force=f(Depth).

So, before plotting, you need to cut off air signal from snow signal to get the snow surface? I suggest to specify what are you talking about here. - To indicate better my confusion: you mean that the penetration depth, let's call it D, is obtained from raw force-distance signal:  $0.0036 = \int_0^D F(z) dz$  so this D stands for what? Does this penetration depth correspond to air/snow interface, or is it somehow related to the weak layer through wf? The lower boundary is fixed or sliding?

*To improve clarity we inserted the formula, changed the parameter name of the penetration depth to PS, and specified that the integration starts at the snow surface (lines 159-162).*

p.5834, L18

What was the skier penetration depth and how was it evaluated?

*We improved the description of the evaluation of the skier penetration depth (line 161; also see reply to above comment).*

p.5834, L19-20

I am afraid that without more details it would be hard to reproduce this step of snow compaction in someone's model. You could better explain how it was done. So, the density below the strip of a width  $a$  was assigned with a new density  $300 \text{ kg m}^{-3}$  and thus new modulus  $16 \text{ MPa}$  until some penetration depth (which was not shown explicitly). However, I am not sure how do you realize it numerically - does it involve some 2D changes in the field of density? Since the penetration of plate into snow with corresponding compaction is by itself a topic for a research paper (e.g. Mohamed and others, 1991) more details would help.

*We inserted "..., i.e. density and thickness of slab layers were adjusted." to make it clear that we changed the layer properties before FE modelling (line 199).*

p. 5834, L28

A matter of taste, but nevertheless: would not it be informative (if meaningful) to indicate the range of  $\theta$  giving you the maximum shear stress? Any skiing reader will be interested to learn these numbers.

*Theta is not constant but varies between  $53^\circ$  and  $60^\circ$  for slope angles ranging between  $0^\circ$  and  $50^\circ$ . The corresponding figure can be found in Schweizer (1997). (Schweizer, J., 1997. Contribution on the skier stability index. Internal report, 712, Swiss Federal Institute for Snow and Avalanche Research, Davos, Switzerland).*

p.5834, L21-22 & p. 5839, L1-3 & p. 5840, L13-15

"A fixed value of the Poisson's ratio . . ." - I am wondering if this could also contribute to predicted values of critical cut length (Sect 3.2). Some studies proposed to use the ratio as a function of density (Sigrist and others, 2006; Sigrist and Schweizer, 2007; Mellor, 1975; Teufelsbauer, 2011). Usually, constant value works well and has little influence, however, usage of some analytical solutions (e.g., Heierli and Zaiser, 2006) shows that the critical crack length can vary for several % as a function of the ratio. Same may be said about roots of your expression (Eq.6). Perhaps, this will be of minor importance in improving the agreement, but nevertheless is worth checking with sensitivity tests for dropping away insignificant factors in future work.

*We agree that the influence of the Poisson's ratio is rather minor. The influence of the Poisson's ratio will not affect the results as the uncertainties involved with SMP-derived snow properties are within 10-20%.*

p. 5835, L5

"slab larger than the ski(er) width (0.2m)." -> ". . . the ski width. . .?"

*We changed to "width of skier load" (line 212).*

p. 5836, L 6

What is  $\gamma$  and how did you select it (same for Eq.7)? It appears to be even more important than Poisson ratio for high slab thickness if varies between 0-2.

*We now specify gamma (lines 229-230) which is the elastic mismatch parameter (Heierli et al., 2008).*

p. 5837, L13

"Eq. (6) is then solved" - with help of what? I recommend to specify your media for this here.

*We clarified in lines 253-254 that we find the exact solution.*

p. 5839, L4

Since the values of the critical cut can vary from 10 to 60 cm it is important to indicate here the relative mean % to highlight how good the agreement actually is.

*We now also provide the mean absolute percentage error (line 290).*

p. 5841, L14-18

Here, I recommend to direct a reader to a work where some steps in this direction have been previously made (e.g., Mahajan and Joshi, 2008).

*We added the reference to Mahajan and Joshi (2008) (lines 351-352).*

p. 5842, L17-19

Even if the approach and its quantitative nature are indeed novel and original contribution, I nevertheless suggest to put some reference here. Because, as far as I know, the necessity of holistic view to snow avalanche release has been in the air for quite some time (e.g. McClung and Schaerer, 2006 or McClung, 2009). So that this sentence reads as something like: "Whereas previous authors noted a need of holistic approach to avalanche initiation [ . . . refs], and we anticipated this finding (i.e. that both conditions have to be fulfilled), we are not aware that it has been demonstrated before." Also, I think it would be honest to mention in Discussion or Conclusions one of the difficulties which may limit a direct utilization of your approach by snow professionals - a need to rely on FEM in order to evaluate skier-induced stresses at weak layer depth,  $\Delta\tau$ , for a given snowpack stratification for obtaining the S. Perhaps, you could also share you vision or idea what to do without this  $\Delta\tau$ ; say, make compromise and rely on analytical solution for a uniform slab (Fig. 4) which is, however, not a good approximation for predicting  $\tau_c$ ?

*We agree that a "holistic" approach is needed for avalanche forecasting, i.e. that one should not make any decisions based on a single in situ test – as pointed out e.g. by McClung (2009). However, we refer to the two important processes in avalanche release – failure initiation and crack propagation – to be considered in point stability estimation.*

*To this end, McClung and Schaerer (2006) clearly stated that the appropriate measure for assessing snow slope instability is considering the balance between a shear stress intensity factor and shear fracture toughness (p. 80). In other words, they consider propagation as the only decisive factor since dry slab avalanches initiate by propagating shear fractures.*

*We are of course aware that it is always a long way into practice but we are convinced that today it is time for more sophisticated approaches that include numerical simulations – and many people carry a smartphone with sufficient computing power these days. So maybe we're able to model the  $\Delta\tau$  right away in the field in future.*

### **Cited references**

- Heierli, J. and Zaiser, M. (2006). An analytical model for fracture nucleation in collapsible stratifications. *Geophysical Research Letters*, 33: 06501.
- Mahajan P and Joshi SK (2008) Modeling of interfacial crack velocities in snow. *Cold Reg. Sci. Technol.*, 51(2–3), 98–111, doi: 10.1016/j.coldregions.2007.05.008
- Mellor M (1975) A review of basic snow mechanics. IAHS Publ. 114 (Symposium at Grindelwald 1974 – Snow Mechanics), 251–291
- McClung, D. M. and Schaerer, P.: *The Avalanche Handbook*, The Mountaineers Books, Seattle WA, USA, 2006.
- McClung, D. M. (2009), Dry snow slab quasi-brittle fracture initiation and verification from field tests, *J. Geophys. Res.*, 114, F01022, doi:10.1029/2007JF000913.
- Mohamed AMO, Yong RN and Murcia AJ (1991) Evaluation of the performance of deep snowpack under compression loading using finite element analysis. *J. Terrmech.*, 30(4), 219–257 (doi: 10.1016/0022-4898(93)90013-N)
- Teufelsbauer H (2011) A two-dimensional snow creep model for alpine terrain. *Natur. Hazards*, 56(2), 481–497 (doi: 10.1007/s11069-010-9515-8)

## Reply to Referee #2 (Bruce Jamieson) RC C3160 / SC C2799

### General comments

An excellent contribution. Well argued and very well referenced.

### Specific comments

The relationship between critical crack length and crack propagation propensity could be clearer. Shorter cut lengths in PST tests (assumed similar to critical crack lengths) are not simply e.g. inversely, related to crack propagation propensity.

In various papers, Gauthier related validated propagation propensity to cut lengths less than 50% of column length AND crack propagation to the end of the column in a PST test. Statements such as in lines 3-4 of page 5829 oversimplify criticality. One way to clarify this is to define criticality not simply in terms of the start of propagation but propagation over a distance on the scale of 1 m.

*We agree that Gauthier and Jamieson (2008) combined a threshold of critical crack length with the experimental PST fracture result to define crack propagation propensity and now describe this in more detail (lines 53-56).*

*Here we used a dataset of fully propagating PSTs with beams longer than 120 cm and critical crack lengths of up to 60 cm (corresponding well to previously published suggestions) to compare our model results with. Further we seek to derive a critical value for modeled crack lengths by comparing our model results with presence of signs of instability. We report a value of the critical crack length of 40 cm which is below Gauthier's suggestion (of below half the column length) given a column length of 120 cm, which is the shortest column length in our data.*

Page 5833 lines 10-15. Some clarification of the failure mode in the stability criterion is needed. The shear stress term in the denominator is traditionally slope parallel e.g. Habermann et al. (2008), but this is not the case for strength derived from the SMP (numerator in Eq 5.), which is "an indentation test". A statement that "slope-parallel shear strength over shear stress is not being used because . . ." would be helpful.

*We added the following sentence (lines 173-175):*

*"... , i.e. we cannot use the slope-parallel shear strength because the SMP is an indentation test measuring an effective strength resulting from the mixed-mode breaking of bonds at the tip."*

Page 5835 line 5 "the FE model reproduced the maximum shear stress very well . . . R2 = 0.94." How do the intercepts from the two methods compare? A statement about the intercepts or a graph would help.

*We now provide information on the regression slope for a linear regression of the shear stress derived with the finite element and the analytical solution (regression slope  $m = 1.20$ ) instead of providing the intercepts of the regression, as the solution does not converge for finite depths (line 212)*

Page 5837 line 5 – 14: If the deflecting beam is never supported by closing the gap between the slab and the bed surface, say so, and note that this may be different from real slab bending over collapsing weak layers.

*We agree and added the following sentence (lines 250-251):*

*"In our model, the deflecting beam never got in touch with the basal layer, which, however, may be the case in field experiments, in particular with soft slabs."*

Technical comments on clarity & presentation Page 5831 line 18: hand hardness index for each manually identified layer.

*We inserted in line 134 as suggested: "... for each manually identified layer..."*

Page 5833 line 23-24: presumably this because snow is much more sensitive to dynamic stress than quasi static stress. This is worth mentioning.

*We agree that the rate of loading might explain part of the difference between SMP-derived strength and shear strength measured with the shear frame, but also the type of loading and the sample size probably contribute to the difference.*

Page 5835 line 5: Replace "skier" with something like "combined width of two skis" or "width of skier load"

*We changed the wording in line 212 as suggested.*

Figure 4 and 6: Some fonts are too small.

*We increased the font size in Figs. 4a and 6a.*

## **Additional changes**

Apart from the above changes we also changed the following lines to ensure clarity and consistency.

Line 74: "linear elastic" inserted to stress differences in modeling assumptions with subsequent statement

Line 147: Reference updated.

Line 196: Parameter name of the strip load changed to  $P$  to avoid confusion with penetration resistance  $F$ .

Lines 302 to 308: Classification tree analysis performed for both criteria for better transparency. Reference inserted to refer to comparable, previously published values.

Line 324: Reference updated.

Line 376: Inserted "to the best of our knowledge".

Line 388-389: Inserted "We are grateful for the constructive review comments by E. Podolskiy and B. Jamieson."

Line 436-437: Reference inserted.

Line 440-441: Reference inserted.

Line 449: Reference inserted.

Line 456-458: Reference edited and updated.

Line 483-484: Reference updated.

Figure 4a: Parameter name of the strip load changed to  $P$  to avoid confusion with penetration resistance  $F$ .

Line 515: Parameter name of the strip load changed to  $P$  to avoid confusion with penetration resistance  $F$ .

Line 520: Inserted "solid".

Line 534: "dotted" changed to "dashed".

Line 541: "dotted" changed to "dashed".

Line 541-542: Derivation of split values (lines in graph) addressed.

# A process-based approach to estimate point snow instability

Benjamin Reuter, Jürg Schweizer, Alec van Herwijnen

WSL Institute for Snow and Avalanche Research SLF, Flüelastrasse 11, 7260 Davos Dorf, Switzerland

1 **Abstract:** Snow instability data provide information about the mechanical state of the snow cover  
2 and are essential for forecasting snow avalanches. So far, direct observations of instability (recent  
3 avalanches, shooting cracks or whumpf sounds) are complemented with field test such as the  
4 rutschblock test, since no measurement method for instability exists. We propose a new approach  
5 based on snow mechanical properties derived from the snow micro-penetrometer that takes into  
6 account the two essential processes during dry-snow avalanche release: failure initiation and crack  
7 propagation. To estimate the propensity of failure initiation we define a stress-based failure  
8 criterion, whereas the propensity of crack propagation is described by the critical cut length as  
9 obtained with a propagation saw test. The input parameters include layer thickness, snow density,  
10 effective elastic modulus, strength and specific fracture energy of the weak layer – all derived from  
11 the penetration-force signal acquired with the snow micro-penetrometer. Both instability measures  
12 were validated with independent field data and correlated well with results from field tests.  
13 Comparisons with observed signs of instability clearly indicated that a snowpack is only prone to  
14 avalanche if the two separate conditions for failure initiation and crack propagation are fulfilled. To  
15 our knowledge, this is the first time that an objective method for estimating snow instability has  
16 been proposed. The approach can either be used directly based on field measurements with the  
17 snow micro-penetrometer, or be implemented in numerical snow cover models. With an objective  
18 measure of instability at hand, the problem of spatial variations of instability and its causes can now  
19 be tackled.

## 20 1 Introduction

21 Snow slope stability describes the mechanical state of the snow cover on an inclined slope and is  
22 inversely related to the probability of avalanche release (McClung and Schaerer, 2006). For a given  
23 time, depth within the snowpack, and location on a slope, snow stability can be described as the  
24 balance between snow strength and stress termed stability index (Roch, 1966). This index has been  
25 widely used (e.g. Conway and Abrahamson, 1984; Perla et al., 1982) and refined by taking into  
26 account triggering by an additional load such as a skier (Föhn, 1987). Whereas, the skier stability  
27 index has been shown to be related to the probability of skier triggering (Jamieson, 1995), this critical  
28 stress approach does not take into account that slope failure requires crack propagation. While  
29 failure initiation may depend on stress only, the propagation of cracks requires deformation energy  
30 (Bazant and Planas, 1998). Furthermore, on a slope, strength and stress are spatially variable; these  
31 variations are fundamental to the fracture process (Schweizer et al., 2003). Around locally failed  
32 areas stress concentrations will form and drive crack propagation, and eventually cause catastrophic  
33 failure before the average material strength is reached. This observation has been termed knock-  
34 down effect (Fyffe and Zaiser, 2004) and partly explains why the stability index derived from  
35 measurements at or near natural slab avalanches often indicated stable conditions ([Perla, 1977](#)).



36 Not surprisingly, the link between point observations of snow stability and snow slope stability is not  
37 clear, yet (e.g. Bellaire and Schweizer, 2011). Scale issues due to different measurement scales, the  
38 so-called support and knowledge gaps between the processes involved at both scales have  
39 complicated bringing together point and slope scale snow instability results (Schweizer et al., 2008a).  
40 The point stability scale is not even well defined. Failure initiation refers to the collective failing of  
41 snow grains, or bonds between grains, on the scale of centimeters and the onset of a self-  
42 propagating crack in a weak snow layer called crack propagation. A common scale for both processes  
43 is the snowpack scale which spans about one square meter (Schweizer and Kronholm, 2007) which in  
44 the following we will refer to when we use the term point snow instability.

45 The stability index assumes a transition from stable to unstable when driving forces are no longer  
46 balanced by resisting forces. However, this approach is questionable, primarily since dry-snow slab  
47 avalanche release is the result of a series of fractures and snow properties are spatially variable. In a  
48 fracture mechanical view, to describe a material's resistance to crack propagation, flaw size and  
49 toughness need to be considered additionally to the stresses (Anderson, 1995). With the  
50 introduction of the propagation saw test (PST) (Gauthier and Jamieson, 2006; Sigrist and Schweizer,  
51 2007) all these properties can be obtained from field data. PST experiments to study propagating  
52 cracks have confirmed deformation of the slab to substantially contribute to the mechanical energy  
53 consumed by crack extension (van Herwijnen et al., 2010). Further, Gauthier and Jamieson (2008b)  
54 have shown that the critical crack length together with the fracture result are related to slope  
55 instability. In particular, cracks propagating to the end of the column after saw cut lengths less than  
56 50 % of the column length were clear indicators of high crack propagation propensity.

57 There is presently no objective measurement of snow instability. Instead, recent avalanches,  
58 whumpfs or shooting cracks are considered indicators of instability (Jamieson et al., 2009), but these  
59 observations are rare. In their absence the remaining option to gather field data on snow instability is  
60 snow instability testing (Schweizer and Jamieson, 2010). The rutschblock (RB) is a traditional snow  
61 stability test (Schweizer, 2002). The RB score was found indicative of the failure initiation propensity,  
62 the RB release type of the crack propagation propensity (Schweizer et al., 2008b). Whereas the RB  
63 release type only represents an ordinal rank, the propagation saw test (PST) gives a metric value, the  
64 critical cut length, which eases quantitative analysis. A combination of the results of both tests  
65 therefore seems appropriate for snow instability assessment.

66 Several studies focused on snow instability in the past, thereby either concentrating on failure  
67 initiation or crack propagation. Both, Bellaire et al. (2009) and Pielmeier and Marshall (2009) derived  
68 stability related parameters from measured snow micro-penetrometer resistance profiles. They  
69 found that weak layer strength and average slab density predicted with good accuracy stability  
70 classes estimated from RB tests.

71 Under the assumption of a uniform slab on a rigid substratum Heierli (2008) presented estimates of  
72 critical crack lengths obtained from recalculation of PST field experiments. Yet, averaging slab  
73 properties is a strong simplification and Schweizer (1993) pointed out the importance of slab  
74 properties for failure initiation. By means of linear elastic finite element (FE) simulations of typical  
75 snow profile types Habermann et al. (2008) found the stress at the depth of the weak layer to vary by  
76 a factor of two compared to a uniform slab. McClung (2009) suggested an alternative model to  
77 estimate the critical crack length by considering a finite fracture process zone.

78 Several numerical approaches focusing on avalanche release (for a summary see Podolskiy et al.,  
79 2013) have been made but only a few incorporate both fracture processes. Among the latest were  
80 Gaume et al. (2013) who presented a Mohr-Coulomb failure criterion based model taking into  
81 account variations of weak layer shear strength and stress redistribution by slab elasticity. Only  
82 lately, a possible refinement of the classical stability index by accounting for strength variations and  
83 their knock-down effect including a derivation of a critical crack length was presented (Gaume et al.,  
84 2014).

85 Predicting snow instability requires snow properties obtained either from field measurements or  
86 from snow cover modeling. In the field, the method of choice is the snow micro-penetrometer (SMP)  
87 (Schneebeli and Johnson, 1998) that allows deriving microstructural and micromechanical properties  
88 from the penetration force-distance signal (Johnson and Schneebeli, 1999). Marshall and Johnson  
89 (2009) showed that values of snow density, elastic modulus and strength derived from snow micro-  
90 penetrometer signals compared well with literature data. Interpreting the oscillation of the  
91 penetration force as a Poisson shot-noise process Löwe and van Herwijnen (2012) suggested a more  
92 robust method to extract the microstructural parameters. Their method was employed by Proksch et  
93 al. (2014) who developed a reliable parameterization of snow density applicable to a wide range of  
94 snow types. Reuter et al. (2013) showed that with the snow micro-penetrometer apart from snow  
95 density and effective modulus also the specific fracture energy of the weak layer can be derived.  
96 Comparing the results for mechanical properties obtained with snow micro-tomography (Schneebeli,  
97 2004) to those with particle tracking velocimetry of propagation saw tests (van Herwijnen et al.,  
98 2010) they substantiated the reliability of SMP-derived parameters.

99 Alternatively, snow cover models provide snow structural information allowing snow instability  
100 modeling (Durand et al., 1999; Lehning et al., 2004). However, snow mechanical properties are often  
101 not simulated independently, but parameterized on density only. Schweizer et al. (2006) refined the  
102 skier's stability index implemented in the snow cover model SNOWPACK and validated it with field  
103 observations. By first identifying the potential weakness in a simulated profile and then assessing its  
104 stability Monti et al. (2014) improved this approach to classify profiles into three classes of snow  
105 instability: poor, fair and good.

106 Given the fracture mechanical context of dry-snow slab avalanche release and the lack of an  
107 objective measure of instability, we propose that a description of instability should take into account  
108 the two essential processes in slab avalanche release, i.e. failure initiation and crack propagation,  
109 and be based on snow mechanical properties measured with the snow micro-penetrometer. Our goal  
110 is to provide an observer-independent methodology applicable to field measurements of snow  
111 stratigraphy. To this end we introduce a two-step calculation of a stability criterion and a critical  
112 crack length based on snow mechanical properties measured with the SMP. Then, we will validate  
113 the performance of our approach with field experiments of snow instability. Finally, we will show  
114 how classical snow instability observations may be interpreted in terms of failure initiation and crack  
115 propagation.

## 116 **2 Methods**

117 First, we present the experimental data, and then we describe how the mechanical field data  
118 acquired with the snow micro-penetrometer was analyzed, before we introduce the new approach  
119 to derive snow instability.

## 120 2.1 Field data

121 Two datasets of SMP measurements were exploited to test the performance of the failure initiation  
122 (A) and the crack propagation (B) part of our approach. Dataset A was originally presented by Bellaire  
123 et al. (2009). As meta data on snow instability was only available for a share of the data, 64 SMP  
124 measurements were kept for further analysis. They were all performed in close proximity (<0.5 m) to  
125 a RB test. The main results of a RB test, which is a point observation, are score and release type  
126 (Figure 1). We used the score for validating the failure initiation propensity (Schweizer and Jamieson,  
127 2010).

128 Dataset B consists of 31 SMP measurements which have been performed in a distance less than  
129 30 cm from the lower end of the column of propagation saw tests (PST) (Figure 2). Data were  
130 collected on seven different days. We filmed the fractures in the PSTs to precisely determine the  
131 onset of propagation by measuring the critical cut length in the pictures as a criterion of crack  
132 propagation.

133 Both datasets also include manually observed snow profiles including snow grain type and size and  
134 hand hardness index [for each manually identified layer](#). In addition, 77 out of the 95 field records in  
135 total contain information on either type or absence of signs of instability.

## 136 2.2 Snow micro-penetrometer

137 With the snow micro-penetrometer (SMP) a penetration resistance profile is recorded to a depth  
138 well below the weak layer at sub-millimeter resolution. Based on the detailed manually observed  
139 snow profile layers were defined from the corresponding sections of the signal, namely slab layers, a  
140 weak layer and a basal layer. As every layer is later represented in a finite element (FE) model and  
141 the resolution of the SMP is higher than the one needed for FE simulations, we deal with layers for  
142 the sake of shorter computation times. Figure 3 shows an example of a SMP signal with manually  
143 assigned snow layer boundaries.

144 Applying the shot-noise model by Löwe and van Herwijnen (2012) snow micro-structural parameters,  
145 namely the rupture force  $f$ , the deflection at rupture  $\delta$  and the structural element size  $L$  were  
146 calculated over a moving window  $w$  of 2.5 mm with 50% overlap and then averaged over the layer.  
147 Snow density was calculated as described in Proksch et al. (2015):

$$148 \rho = a_1 + a_2 \log(\tilde{F}) + a_3 L \log(\tilde{F}) + a_4 L \quad (1)$$

149 where  $a_i$  are coefficients,  $F$  is the penetration resistance and tilde denotes the median. The micro-  
150 mechanical effective modulus and strength were calculated according to Johnson and Schneebeli  
151 (1999):

$$152 E = \frac{f}{\delta L} \quad (2)$$

153 and

$$154 \sigma = \frac{f}{L^2} \quad (3)$$

155 The specific fracture energy of the weak layer (WL) was calculated as the minimum of the  
156 penetration resistance integrated across the window size  $w$  within the weak layer (Reuter et al.,  
157 2013):

158  $w_f = \min_{WL} \int_{-\frac{w}{2}}^{+\frac{w}{2}} F dz .$  (4)

159 The penetration depth PS was derived by integrating from the snow surface over the penetration  
 160 resistance F to a threshold absorbed energy  $e_a = 0.0036$  J, which had been determined by comparison  
 161 of SMP profiles with concurrently observed penetration depth (Schweizer and Reuter, 2015):

162  $e_a = \int_0^{PS} F(z) dz.$  (5)

163 **2.3 Modeling**

164 In the following the modeling approach to calculate estimates of the failure initiation and the crack  
 165 propagation propensity of a certain slab-weak layer combination is described and validated. The  
 166 mechanical properties required as input are obtained from the SMP signal as described above.

167 *2.3.1 Failure initiation*

168 A strength-over-stress criterion *S* describes the propensity of the weak layer to fail in the case of an  
 169 additional load:

170  $S = \frac{\sigma_{WL}}{\Delta\tau},$  (6)

171 with  $\sigma_{WL}$  being the strength of the weak layer and  $\Delta\tau$  being the maximum additional shear stress at  
 172 the depth of the weak layer due to skier loading. The strength of the weak layer is approximated by  
 173 the micro-mechanical strength derived from the snow micro-penetrometer signal in the weak layer,  
 174 i.e. we cannot use the slope-parallel shear strength because the SMP is an indentation test  
 175 measuring an effective strength resulting from the mixed-mode breaking of bonds at the tip. The  
 176 maximum shear stress at the depth of the weak layer was modeled with the 2D linear elastic finite  
 177 element (FE) model originally designed by Habermann et al. (2008) to calculate the shear stress at  
 178 the depth of the weak layer below a layered slab due to the weight of a skier. *S* may be interpreted  
 179 as an indicator of failure initiation with low (high) values being associated with high (low) likelihood  
 180 of initiating a failure. Note, the stability criterion *S* is not expected to yield typical values of the skier's  
 181 stability index (< 1 for 'unstable', > 1.5 for 'stable') (Jamieson and Johnston, 1998). One reason is that  
 182 SMP-derived strength values are about two orders of magnitude larger than values of shear strength  
 183 reported in literature (Marshall and Johnson, 2009) as the SMP measurement is an indentation test.

184 The 2D FE model by Habermann et al. (2008) has been adopted to include all relevant slab layers –  
 185 usually about 5 to 10 layers. The geometry of the model (Figure 4a) was chosen such that the length  
 186 of the modeled section of the snowpack (10 m) is at least one order of magnitude larger than the  
 187 average depth of the weak layer to keep boundary effects small. The model consists of multiple  
 188 layers including slab and basal layers as well as an embedded weak layer corresponding to the  
 189 layering identified in the SMP signal. The layers are inclined by the slope angle  $\alpha$ . Nodes at the lower  
 190 end (on the right of Figure 4a) and at the snow soil interface were fixed in both coordinate directions.

191 The model domain was divided into two-dimensional, quadrilateral plane strain elements having  
 192 eight nodes each. The mesh consisted of 75 nodes in the horizontal and 100 nodes in the vertical per  
 193 meter. The model has been implemented in ANSYS workbench to calculate the maximum shear  
 194 stress within the weak layer. We assumed plane strain as stresses in the direction normal to the x-y

195 plane are smaller than within and linear elastic behavior as the loading rate is high considering skier  
 196 loading. The skier load was modeled as a static strip load  $\underline{P}$  of 780 N spread over a width  $a$  of 0.2 m.  
 197 To account for skier penetration we assumed the layers within the penetration depth to be  
 198 compacted to a density of  $300 \text{ kg m}^{-3}$  with a corresponding elastic modulus of 16 MPa according to  
 199 Scapozza (2004), i.e. density and thickness of slab layers were adjusted. All snow layers in the FE  
 200 model were assigned thickness, density and effective modulus values as derived from the SMP signal.  
 201 A fixed value of the Poisson's ratio was chosen ( $\nu = 0.25$ ). From the modeled linear elastic behavior  
 202 the maximum shear stress within the weak layer was computed yielding  $\Delta\tau$  of Eq. 6, i.e. not  
 203 considering the stress due to the weight of the slab.

204 The FE model was tested to reproduce the analytical solution of McClung and Schweizer (1999) for  
 205 the shear stress for a strip load on a finite area  $\tau(\theta, H)$  where  $\theta$  and  $H$  are two-dimensional polar  
 206 coordinates. To do so, the maximum shear stress at a certain depth  $H$  was determined by varying  $\theta$ .  
 207 The FE model was run with a Poisson's ratio of  $\nu = 0.49$ , as the analytical solution assumes an  
 208 incompressible half space. The slab was not stratified, but uniform having a density of  $200 \text{ kg m}^{-3}$ .  
 209 Hence, the solution is independent of the elastic modulus. The simulation results for different slab  
 210 thickness  $H$  are presented in Figure 4b together with the analytical solution. The FE model  
 211 reproduced the maximum shear stress as obtained with the analytical solution very well ( $R^2 = 0.94$ ,  
 212 regression slope  $m = 1.2$ ) especially for slab depth larger than the width of skier load (0.2 m).

### 213 2.3.2 Crack propagation

214 In order to estimate the crack propagation propensity the critical crack length as measured in a PST  
 215 experiment was calculated for a weak layer embedded by a layered slab and a basal layer.

216 A theoretical expression (Eq. 7) linking the fracture energy of the weak layer, the elastic modulus of  
 217 the slab and the critical crack length for a self-propagating crack is obtained by replacing the  
 218 mechanical energy in Griffith's criterion with the total energy of the slab weak layer system found by  
 219 (Heierli, 2008) and was presented in detail by Schweizer et al. (2011). The formulation of the total  
 220 mechanical energy of the slab-weak layer system has been proven to describe the released  
 221 mechanical energy of the slab in a PST reasonably well (van Herwijnen et al., 2010).

$$222 \quad w_f(E, r_c) = \frac{H}{2E} \left[ w_0 + w_1 \frac{r_c}{H} + w_2 \left( \frac{r_c}{H} \right)^2 + w_3 \left( \frac{r_c}{H} \right)^3 + w_4 \left( \frac{r_c}{H} \right)^4 \right], \quad (7)$$

223 with

$$w_0 = \frac{3\eta^2}{4} \tau^2,$$

$$w_1 = \left( \pi\gamma + \frac{3\eta}{2} \right) \tau^2 + 3\eta^2 \tau\sigma + \pi\gamma\sigma^2,$$

$$w_2 = \tau^2 + \frac{9\eta}{2} \tau\sigma + 3\eta^2 \sigma^2,$$

$$w_3 = 3\eta\sigma^2,$$

$$w_4 = 3\sigma^2,$$

224 and  $\tau = -\rho g H \sin(\alpha)$  the shear stress,  $\sigma = -\rho g H \cos(\alpha)$  the normal stress,  $\gamma = 1$  the elastic mismatch  
 225 parameter,  $\eta = \sqrt{4(1 + \nu)/5}$  and  $\nu = 0.25$ . Provided the elastic modulus  $E$ , the density  $\rho$  and the  
 226 thickness of the slab  $H$ , the fracture energy of the weak layer  $w_f$ , and the slope angle  $\alpha$  are known,  
 227 the calculation of the critical crack length  $r_c$  reduces to finding the roots of Eq. 7. This fourth degree

228 polynomial of  $r_c$  has real, ever positive coefficients. Figure 5 illustrates the dependence of the  
 229 polynomial's discriminant on slab thickness and density, which is the case if a dependence of the  
 230 elastic modulus on density is assumed. As the polynomial's discriminant does not change sign for  
 231 typical values of density (and the elastic modulus), solutions consist of a pair of complex conjugated  
 232 and two real roots. A physically meaningful solution of  $r_c$  is obtained, if the complex roots and the  
 233 one with an unexpected sign are discarded.

234 To relax the assumption of a uniform, i.e. not stratified, slab a FE model was designed to determine  
 235 the equivalent bulk modulus  $E'$  of a stratified slab (Figure 6a). The model performed a stepwise  
 236 calculation of the mechanical strain energy  $M$  of a stratified slab due to bending over an increasing  
 237 crack of length  $r$ . In order to recover an equivalent bulk modulus  $E'$ , in a next step the pairs of  
 238 mechanical energy and crack length ( $M$ ,  $r$ ) were fitted with a theoretical expression of the total  
 239 mechanical energy of the slab  $M$  (Heierli, 2008):

$$240 \quad M(E', r) = -\frac{\pi\gamma r^2}{4E'}(\tau^2 + \sigma^2) - \frac{r^3}{6E'H}[\lambda_{\tau\tau}\tau^2 + \lambda_{\sigma\tau}\tau\sigma + \lambda_{\sigma\sigma}\sigma^2], \quad (8)$$

241 with

$$242 \quad \lambda_{\tau\tau} = 1 + \frac{9}{4}\eta\left(\frac{r}{H}\right)^{-1} + \frac{9}{4}\eta^2\left(\frac{r}{H}\right)^{-2},$$

$$243 \quad \lambda_{\tau\sigma} = \frac{9}{2}\eta + \frac{9}{2}\eta^2\left(\frac{r}{H}\right)^{-1},$$

$$244 \quad \lambda_{\sigma\sigma} = 3\eta^2 + \frac{9}{4}\eta\frac{r}{H} + \frac{9}{5}\left(\frac{r}{H}\right)^2.$$

245 The FE model consists of stratified layers, which were assigned SMP-derived values of density,  
 246 effective modulus and thickness (Figure 6a). The Poisson's ratio was kept constant ( $\nu = 0.25$ ). Due to  
 247 its geometry (only considering slab layers) and boundary conditions (rigid support along the ligament  
 248 length ( $L-r$ )) the FE model only considers the behavior of the slab layers as described with the  
 249 formulation of the total mechanical energy of the slab-weak layer system, neglecting deformation in  
 250 the weak or basal layers. In our model, the deflecting beam never got in touch with the basal layer,  
 251 which, however, may be the case in field experiments, in particular with soft slabs. The FE model  
 252 reproduced the theoretical formulation very well ( $R^2 = 0.85$ ), especially for crack lengths  $r$  greater or  
 253 equal the thickness of the overlying slab  $H$  (Figure 6b). With the bulk equivalent modulus  $E'$ , we find  
 254 the exact solution of Eq. 7 and receive the critical crack length  $r_c$  for the specific slab-weak layer  
 255 combination.

## 256 3 Results

257 In the following both model parts predicting the propensity of the snowpack to failure initiation and  
 258 crack propagation are evaluated with the two independent data sets (A and B).

### 259 3.1 Failure initiation

260 For each of the 66 SMP profiles with corresponding RB test (dataset A) the failure initiation criterion  
 261  $S$  was calculated. SMP-derived density, effective modulus, strength and layer thickness were used to  
 262 drive the FE model. For the comparison with the RB score we grouped scores 1 and 2 as well as 6 and  
 263 7 because scores 1 and 7 were observed infrequently. The criterion  $S$  increased with increasing RB  
 264 score (Figure 7a). If for a given  $S$  there was no overlap of the boxes, the predictive power of  $S$  would

265 obviously be very good. Although this is not the case, the medians of the failure initiation criterion  
266 (indicated by gray lines) per RB score increased monotonically with increasing RB scores. This  
267 monotonic increase is reflected in a high Spearman rank correlation coefficient ( $r_s > 0.9$ ). If results are  
268 grouped by scores in two stability classes of  $RB < 4$  and  $RB \geq 4$ , a threshold previously found to  
269 separate lower and higher stability (e.g. Schweizer and Jamieson, 2003), the criterion  $S$  discriminated  
270 well between the two classes (Wilcoxon rank sum test, level of significance  $p = 0.01$ ) with a  
271 classification tree splitting value of  $S = 133$ .

### 272 3.2 Crack propagation

273 All 31 SMP signals from dataset B were analyzed and the critical cut length  $r_c$  was calculated from  
274 Eq. 7 with SMP-derived mechanical properties being density, effective modulus, specific fracture  
275 energy and layer thickness. In Figure 8 the results are contrasted with the critical crack lengths  
276 measured in the field in the PST experiments adjacent to the SMP measurements. On the left  
277 (Figure 8a) model results are shown for the case of a uniform slab, i.e. density and effective modulus  
278 were averaged to show the effect of neglecting the stratigraphy of the slab. Modeled values  
279 overestimated the critical cut length yielding a rather fair Pearson correlation coefficient of  $r_p = 0.58$   
280 and a coefficient of determination of  $R^2 = 0.29$ . Only for a few experiments modeled and observed  
281 crack lengths were similar indicating that assuming a uniform slab is not a good approximation. In  
282 fact, Figure 8b shows that the agreement between model results and observations improved if the  
283 stratification of the slab was taken into account. All identified slab layers were assigned the  
284 corresponding density and effective modulus obtained from SMP signal processing and input in the  
285 FE model to determine the bulk effective modulus of the slab. The modeled values of critical crack  
286 length were clearly related to the measured values ( $r_p = 0.83$ ) as indicated by the collapse of the  
287 linear regression on the 1:1 line (Figure 8b). The regression slope was well-defined ( $p < 0.01$ ) with  
288 some scatter ( $R^2 = 0.50$ ) indicating the uncertainty involved with the presented approach. The critical  
289 crack length was predicted with a root mean squared error of 2 cm, a mean absolute error of 7 cm  
290 and a mean absolute percentage error of 9%.

### 291 3.3 Validation with signs of instability

292 Model results were further compared with independent field observations of signs of instability such  
293 as whumpfs, shooting cracks and recent avalanches. Both datasets (A and B) included records of such  
294 field observations which we grouped in three categories: whumpfs, shooting cracks with or without  
295 whumpfs ('cracks') or 'all signs' (whumpfs, cracks and recent avalanches), i.e. fresh avalanches were  
296 only observed simultaneously with whumpfs and cracks (Figure 9). To jointly relate our modeled  
297 estimates of instability to the observations of instability we contrasted the propensity to crack  
298 propagation, i.e. modeled critical crack length, and failure initiation, i.e. initiation criterion  $S$ , in  
299 Figure 9. Signs of instability were primarily present in the lower left of Figure 9, i.e. for low values of  
300 the failure initiation criterion and the critical crack length. Vice versa no signs of instability were  
301 reported if both criteria yielded high values (upper right). This finding suggests that both criteria, the  
302 one for failure initiation and the one for crack propagation, are linked to snow instability. A  
303 classification tree with the two independent variables  $S$  and  $r_c$  yielded splits of  $S = 234$  and  $r_c = 0.41$  m  
304 which separate between the cases with and without concurrently observed signs of instability (Figure  
305 9). These thresholds divide the plot into four quadrants. In the lower left quadrant all 35 cases with



306 signs of instability as well as ten cases without signs of instability were found. Our split value ( $S=234$ )  
307 for the initiation criterion  $S$  is very similar to the one found by Schweizer and Reuter (2015) who  
308 reported a value of 212. In regard to the modeled critical crack length, Gauthier and Jamieson  
309 (2008a) suggested a value of <50% of the column length which in their study corresponded to 50 cm.  
310 Assuming crack propagation to be likely (two lower quadrants) or failure initiation to be easy (two  
311 left quadrants) does not distinguish sharply between signs of instability present or absent. However,  
312 if both criteria had low values unstable snow conditions were observed (lower left quadrant).

## 313 **4 Discussion**

314 In our present understanding avalanche release is seen as a sequence of fractures. To capture the  
315 two most important steps preceding the detachment of a snow slab we addressed the stress at the  
316 depth of a potential weakness with the failure initiation criterion  $S$  and the critical crack size for self-  
317 propagation with the critical crack length  $r_c$ . We presented a model approach to derive both  
318 quantities from snow micro-penetrometer signals which is a fast method to acquire information on  
319 mechanical properties in the field.

320 Assessing the performance of the model approach with two different field tests (RB and PST) yielded  
321 plausible results. However, the main source of uncertainty is related to the mechanical properties  
322 needed as input for the model. Snow density, effective modulus and specific fracture energy were all  
323 determined from SMP measurements. Uncertainties related to the determination of these  
324 mechanical properties have recently been addressed by Proksch et al. (2015) and Reuter et al. (2013)  
325 and lie within 10-20% for density and fracture energy. Other SMP error sources are known and so  
326 erroneous signals were identified and discarded. Some errors were user-related such as mechanical  
327 disturbances. Other unavoidable errors such as signal drift due to strong temperature changes in the  
328 snowpack or stick slip of the rod at high snow densities were rare.

329 The SMP-derived failure initiation criterion  $S$  performed well based on the evaluation with  
330 rutschblock tests, yielding a better correlation than the one lately observed by Schweizer and Reuter  
331 (2014) using the compression test. They concluded that the dimensions of the compression test and  
332 the type of loading are not ideal for modeling purposes. While the RB test includes six different  
333 loading steps, the load is only increased twice in a compression test, but numerous taps are  
334 performed within the same loading range. The loading of the RB and consequently the stress exerted  
335 on the weak layer increases monotonically with the score (score four and five have the same load).  
336 This is reflected in the fair discrimination of RB scores four and five with the failure initiation  
337 criterion  $S$ . Furthermore, RB loading steps are ordinal numbers, i.e. they can be ranked, but they do  
338 not follow a known relation with stability. Hence, the stress in the weak layer increases stepwise in  
339 the experiment, whereas the modeled stability is continuous. The boxplots in Figure 7 group  
340 modeled values of failure initiation ( $S$ ) with rutschblock classes. The monotonic increase of the  
341 medians suggests that the criterion  $S$  reflects the propensity of failure initiation in a weak layer below  
342 a layered slab. Correlations of the rutschblock release type were neither significant with the initiation  
343 criterion  $S$  ( $r_s = 0.11$ ,  $p = 0.39$ ), nor with the modeled critical cut length ( $r_s = 0.04$ ,  $p = 0.76$ ).

344 The critical cut length was modeled with an accuracy of a few centimeters (RMSE of 2 cm). It was  
345 shown that the slab layering played an important role in the process of crack propagation. Only with  
346 the introduction of the bulk effective modulus imitating the bending behavior of a layered slab



347 measured critical cut lengths were reproduced with good accuracy (Figure 8). Until now research on  
348 snow instability had mainly focused on weak layer or average slab properties (Bellaire et al., 2009;  
349 Pielmeier and Marshall, 2009). Alternatively, the critical value of the crack length could have been  
350 determined by stepwise increasing the crack length in an FE model until the critical energy release  
351 rate reaches the specific fracture energy of the weak layer. This approach, [comparable to the one by](#)  
352 [Mahajan and Joshi \(2008\)](#), however, was not followed due to its high computational expenses, as  
353 repeated meshing for every single iteration step would be costly.

354 The introduced FE models assumed linear elastic behavior and were confined to two dimensions.  
355 These assumptions are in contrast with our knowledge that snow is a porous medium consisting of a  
356 non-isotropic ice/air matrix, exhibiting plastic, elastic and viscous behavior at the macro scale.  
357 However, as loading rates in RB tests and PSTs are high, linear elastic assumptions are justified – for  
358 the rutschblock test at least at a certain depth below the snow surface. Two dimensional modeling  
359 seems sufficient, as three dimensional modeling is not advantageous due to the lack of experimental  
360 orthotropic material properties at this point of time.

## 361 **5 Conclusions**

362 We have developed a novel approach to determine quantitative estimates of both, the failure  
363 initiation and crack propagation propensity of the snowpack based on mechanical properties derived  
364 from objective snow micro-penetrometer measurements. Based on the current understanding of  
365 dry-snow slab avalanche release it includes the mechanical properties of all relevant layers  
366 embedding the weak layer to make predictions on the propensity of initiating a failure and spreading  
367 the crack in a weak layer within the snowpack. The presented approach is process-based, observer-  
368 independent and relies on measurements of mechanical properties.

369 The performance of the two novel measures of instability has been assessed in comparisons with two  
370 different datasets of field tests (rutschblock and propagation saw test). Both measures of instability,  
371 the stress criterion  $S$  as well as the critical crack length  $r_c$  were well correlated with the results of field  
372 tests. In addition, the importance of slab layering especially with respect to crack propagation has  
373 been shown. The comparison of our modeled estimates of snow instability with field observations of  
374 signs of instability clearly indicated that a snowpack is unstable only in case of high failure initiation  
375 as well as high crack propagation propensity. Whereas we anticipated this finding, i.e. that both  
376 conditions have to be fulfilled, we are not aware, [to the best of our knowledge](#), that it has been  
377 demonstrated before.

378 Recent field studies have frequently focused on identifying spatial variations of snow instability and  
379 its drivers which requires an objective measure of instability – which was so far lacking. With the  
380 observer-independent method we presented taking into account both processes, failure initiation  
381 and crack propagation, it will become possible to resolve causes of spatial snow instability variations.  
382 With respect to operational application in the context of avalanche forecasting our approach can be  
383 employed directly based on field measurements, provided a robust and reliable snow micro-  
384 penetrometer is at hand which in addition allows remote data transfer, or be implemented in  
385 numerical snow cover models.

386 **Acknowledgements**

387 B.R. has been supported by a grant of the Swiss National Science Foundation (200021\_144392). We  
388 thank numerous colleagues from SLF for help with the field work. [We are grateful for the](#)  
389 [constructive review comments by E. Podolskiy and B. Jamieson.](#)

390 **References**

- 391 Anderson, T. L.: Fracture mechanics: fundamentals and applications, CRC Press, Boca Raton, U.S.A.,  
392 1995.
- 393 Bazant, Z. P. and Planas, J.: Fracture and size effect in concrete and other quasibrittle materials, CRC  
394 Press, Boca Raton, U.S.A., 1998.
- 395 Bellaire, S., Pielmeier, C., Schneebeli, M., and Schweizer, J.: Stability algorithm for snow micro-  
396 penetrometer measurements, *J. Glaciol.*, 55, 805-813, 2009.
- 397 Bellaire, S. and Schweizer, J.: Measuring spatial variations of weak layer and slab properties with  
398 regard to snow slope stability, *Cold Reg. Sci. Technol.*, 65, 234-241, 2011.
- 399 Conway, H. and Abrahamson, J.: Snow stability index, *J. Glaciol.*, 30, 321-327, 1984.
- 400 Durand, Y., Giraud, G., Brun, E., Mérindol, L., and Martin, E.: A computer-based system simulating  
401 snowpack structures as a tool for regional avalanche forecasting, *J. Glaciol.*, 45, 469-484, 1999.
- 402 Föhn, P. M. B.: The stability index and various triggering mechanisms, in: Symposium at Davos 1986  
403 – Avalanche Formation, Movement and Effects, IAHS Publ. 162, edited by: Salm, B. and Gubler,  
404 H., International Association of Hydrological Sciences, Wallingford, Oxfordshire, UK, 1987, 195-  
405 214.
- 406 Fyffe, B. and Zaiser, M.: The effects of snow variability on slab avalanche release, *Cold Reg. Sci.*  
407 *Technol.*, 40, 229-242, 2004.
- 408 Gaume, J., Chambon, G., Eckert, N., and Naaim, M.: Influence of weak-layer heterogeneity on snow  
409 slab avalanche release: application to the evaluation of avalanche release depths, *J. Glaciol.*,  
410 59, 423-437, 2013.
- 411 Gaume, J., Schweizer, J., van Herwijnen, A., Chambon, G., Reuter, B., Eckert, N., and Naaim, M.:  
412 Evaluation of slope stability with respect to snowpack spatial variability, *J. Geophys. Res.*, 2014.  
413 doi: 10.1002/2014JF00319, 2014.
- 414 Gauthier, D. and Jamieson, B.: Evaluation of a prototype field test for fracture and failure  
415 propagation propensity in weak snowpack layers, *Cold Reg. Sci. Technol.*, 51, 87-97, 2008a.
- 416 Gauthier, D. and Jamieson, B.: Fracture propagation propensity in relation to snow slab avalanche  
417 release: Validating the Propagation Saw Test, *Geophys. Res. Lett.*, 35, L13501, 2008b.
- 418 Gauthier, D. and Jamieson, J. B.: Towards a field test for fracture propagation propensity in weak  
419 snowpack layers, *J. Glaciol.*, 52, 164-168, 2006.
- 420 Habermann, M., Schweizer, J., and Jamieson, J. B.: Influence of snowpack layering on human-  
421 triggered snow slab avalanche release, *Cold Reg. Sci. Technol.*, 54, 176-182, 2008.
- 422 Heierli, J.: Anticrack model for slab avalanche release, Ph.D. Ph.D., University of Karlsruhe, Karlsruhe,  
423 Germany, 102 pp., 2008.
- 424 Jamieson, B., Haegeli, P., and Schweizer, J.: Field observations for estimating the local avalanche  
425 danger in the Columbia Mountains of Canada, *Cold Reg. Sci. Technol.*, 58, 84-91, 2009.
- 426 Jamieson, J. B.: Avalanche prediction for persistent snow slabs, 1995. Ph.D., Department of Civil  
427 Engineering, University of Calgary, Calgary AB, Canada, 258 pp., 1995.
- 428 Jamieson, J. B. and Johnston, C. D.: Refinements to the stability index for skier-triggered dry slab  
429 avalanches, *Ann. Glaciol.*, 26, 296-302, 1998.

430 Johnson, J. B. and Schneebeli, M.: Characterizing the microstructural and micromechanical properties  
431 of snow, *Cold Reg. Sci. Technol.*, 30, 91-100, 1999.

432 Lehning, M., Fierz, C., Brown, R. L., and Jamieson, J. B.: Modeling instability for the snow cover model  
433 SNOWPACK, *Ann. Glaciol.*, 38, 331-338, 2004.

434 Löwe, H. and van Herwijnen, A.: A Poisson shot noise model for micro-penetration of snow, *Cold Reg.*  
435 *Sci. Technol.*, 70, 62-70, 2012.

436 [Mahajan, P. and Joshi, S.K.: Modeling of interfacial crack velocities in snow, \*Cold Reg. Sci. Technol.\*,  
437 \*51\(2-3\)\*, 98-111, 2008.](#)

438 Marshall, H.-P. and Johnson, J. B.: Accurate inversion of high-resolution snow penetrometer signals  
439 for microstructural and micromechanical properties, *J. Geophys. Res.*, 114, F04016, 2009.

440 [McClung, D. M.: Dry snow slab quasi-brittle fracture initiation and verification from field tests, \*J.\*  
441 \*Geophys. Res.\*, 114, F01022, doi:10.1029/2007JF000913, 2009.](#)

442 McClung, D. M. and Schaerer, P.: *The Avalanche Handbook*, The Mountaineers Books, Seattle WA,  
443 U.S.A., 2006.

444 McClung, D. M. and Schweizer, J.: Skier triggering, snow temperatures and the stability index for dry  
445 slab avalanche initiation, *J. Glaciol.*, 45, 190-200, 1999.

446 Monti, F., Schweizer, J., and Gaume, J.: Deriving snow stability information from simulated snow  
447 cover stratigraphy, *Proceedings ISSW 2014. International Snow Science Workshop, Banff,*  
448 *Alberta, Canada, 29 September - 3 October 2014*, 465-469, 2014.

449 [Perla, R.: Slab avalanche measurements, \*Can. Geotech. J.\*, 14\(2\), 206-213, 1977.](#)

450 Perla, R., Beck, T. M. H., and Cheng, T. T.: The shear strength index of alpine snow, *Cold Reg. Sci.*  
451 *Technol.*, 6, 11-20, 1982.

452 Pielmeier, C. and Marshall, H.-P.: Rutschblock-scale snowpack stability derived from multiple quality-  
453 controlled SnowMicroPen measurements, *Cold Reg. Sci. Technol.*, 59, 178-184, 2009.

454 Podolskiy, E. A., Chambon, G., Naaim, M., and Gaume, J.: A review of finite-element modelling in  
455 snow mechanics, *J. Glaciol.*, 59, 1189-1201, 2013.

456 Proksch, M., Löwe, H., and Schneebeli, M.: Density, specific surface area and correlation length of  
457 snow measured by high-resolution penetrometry, *J. Geophys. Res.*, 120, doi:  
458 [10.1002/2014JF003266](#), 2015.

459 Reuter, B., Proksch, M., Loewe, H., van Herwijnen, A., and Schweizer, J.: On how to measure snow  
460 mechanical properties relevant to slab avalanche release, *Proceedings ISSW 2013.*  
461 *International Snow Science Workshop, Grenoble, France, 7-11 October 2013, 7-11, 2013.*

462 Reuter, B. and Schweizer, J.: The effect of surface warming on slab stiffness and the fracture behavior  
463 of snow, *Cold Reg. Sci. Technol.*, 83-84, 30-36, 2012.

464 Roch, A.: Les déclenchements d'avalanches. In: *Symposium at Davos 1965 - Scientific Aspects of*  
465 *Snow and Ice Avalanches*, IAHS Publication, 69, Int. Assoc. Hydrol. Sci., Wallingford, U.K., 1966.

466 Scapozza, C.: *Entwicklung eines dichte- und temperaturabhängigen Stoffgesetzes zur Beschreibung*  
467 *des visko-elastischen Verhaltens von Schnee*, Ph.D. thesis, Institut für Geotechnik, ETH Zurich,  
468 Zurich, Switzerland, 250 pp., 2004.

469 Schneebeli, M.: Numerical simulation of elastic stress in the microstructure of snow, *Ann. Glaciol.*, 38,  
470 339-342, 2004.

471 Schneebeli, M. and Johnson, J. B.: A constant-speed penetrometer for high-resolution snow  
472 stratigraphy, *Ann. Glaciol.*, 26, 107-111, 1998.

473 Schweizer, J.: The influence of the layered character of snow cover on the triggering of slab  
474 avalanches, *Ann. Glaciol.*, 18, 193-198, 1993.

475 Schweizer, J.: *The Rutschblock test - Procedure and application in Switzerland*, *The Avalanche*  
476 *Review*, 20, 1,14-15, 2002.

477 Schweizer, J. and Jamieson, J. B.: Snowpack properties for snow profile analysis, Cold Reg. Sci.  
478 Technol., 37, 233-241, 2003.

479 Schweizer, J. and Jamieson, J. B.: Snowpack tests for assessing snow-slope instability, Ann. Glaciol.,  
480 51, 187-194, 2010.

481 Schweizer, J. and Kronholm, K.: Snow cover spatial variability at multiple scales: Characteristics of a  
482 layer of buried surface hoar, Cold Reg. Sci. Technol., 47, 207-223, 2007.

483 Schweizer, J. and Reuter, B.: [A new index combining weak layer and slab properties for snow](#)  
484 [instability](#), Nat. Hazards Earth Syst. Sci., [15](#), 109-118, 2015.

485 Schweizer, J., Bellaire, S., Fierz, C., Lehning, M., and Pielmeier, C.: Evaluating and improving the  
486 stability predictions of the snow cover model SNOWPACK, Cold Reg. Sci. Technol., 46, 52-59,  
487 2006.

488 Schweizer, J., Jamieson, J. B., and Schneebeli, M.: Snow avalanche formation, Rev. Geophys., 41,  
489 1016, 2003.

490 Schweizer, J., Kronholm, K., Jamieson, J. B., and Birkeland, K. W.: Review of spatial variability of  
491 snowpack properties and its importance for avalanche formation, Cold Reg. Sci. Technol., 51,  
492 253-272, 2008a.

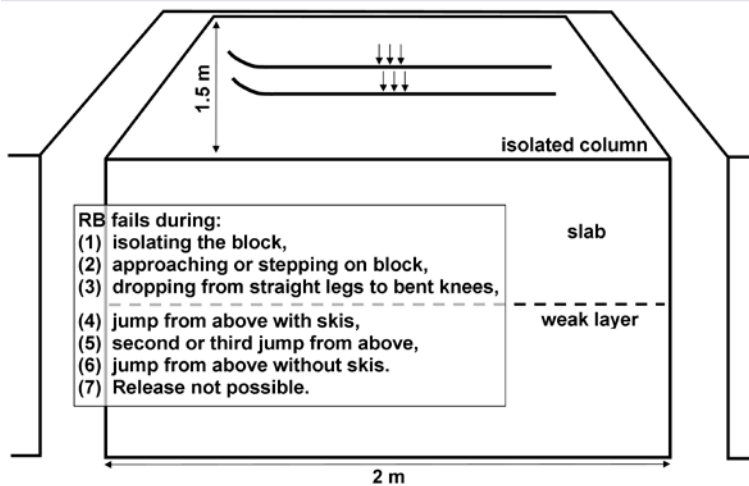
493 Schweizer, J., McCammon, I., and Jamieson, J. B.: Snowpack observations and fracture concepts for  
494 skier-triggering of dry-snow slab avalanches, Cold Reg. Sci. Technol., 51, 112-121, 2008b.

495 Schweizer, J., van Herwijnen, A., and Reuter, B.: Measurements of weak layer fracture energy, Cold  
496 Reg. Sci. Technol., 69, 139-144, 2011.

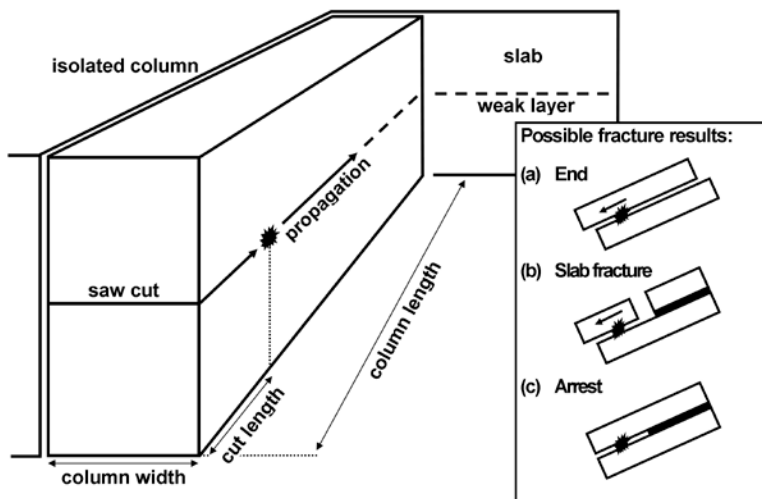
497 Sigrist, C. and Schweizer, J.: Critical energy release rates of weak snowpack layers determined in field  
498 experiments, Geophys. Res. Lett., 34, L03502, doi:03510.01029/02006GL028576, 2007.

499 van Herwijnen, A., Schweizer, J., and Heierli, J.: Measurement of the deformation field associated  
500 with fracture propagation in weak snowpack layers, J. Geophys. Res., 115, F03042,  
501 doi:03010.01029/02009JF001515, 2010.

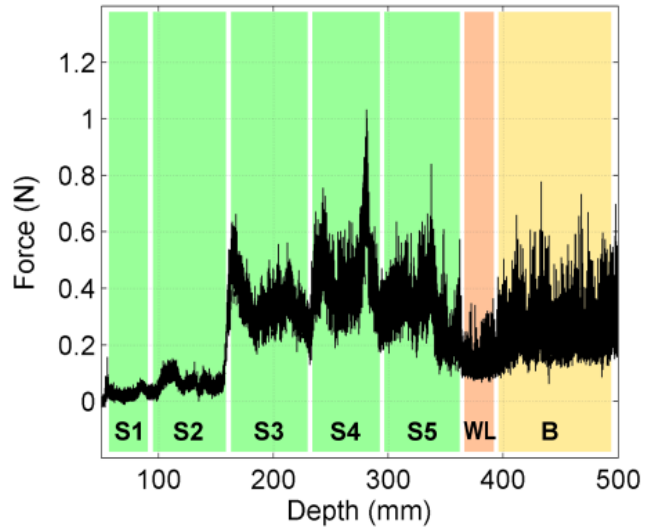
Figure Captions and Figures



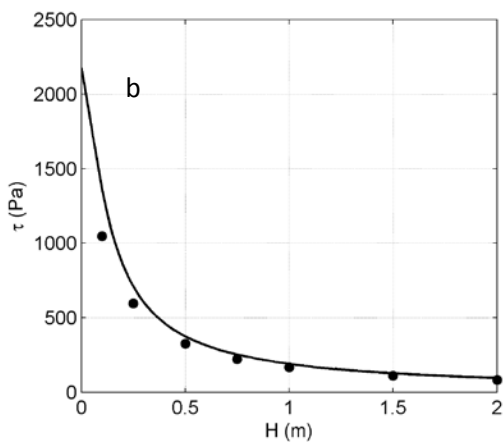
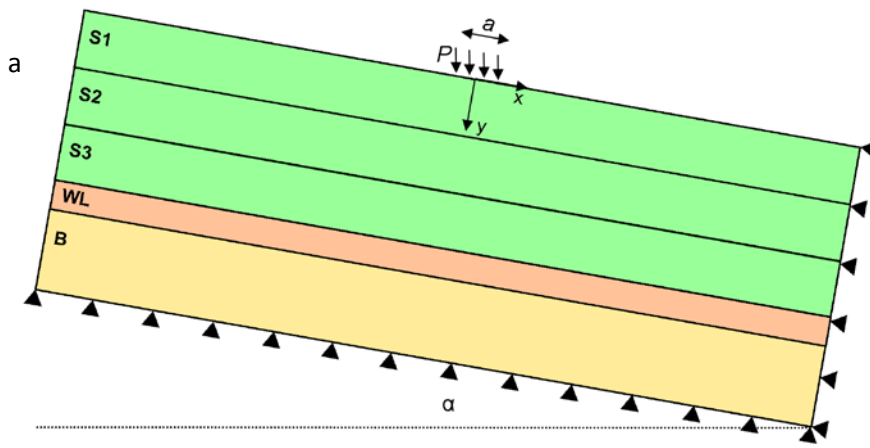
502 Figure 1: Sketch presenting the rutschblock (RB) test as it is seen looking upslope: After isolating a  
 503 block of snow 2 m wide and 1.5 m upslope it is loaded progressively by a skier. The loading steps and  
 504 scores are described in the inset. The release type was not considered here.



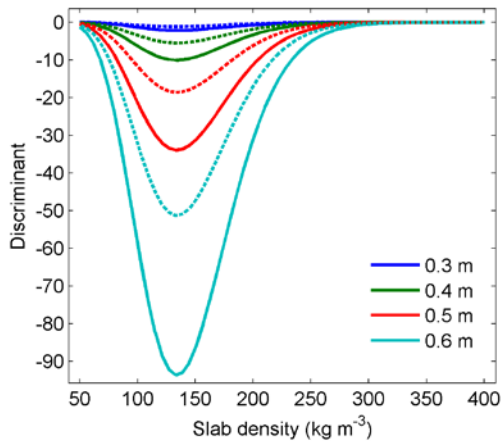
505  
 506 Figure 2: Sketch presenting the propagation saw test (PST) as it is seen looking upslope: After  
 507 isolating a column 30 cm wide and at least 1.2 m upslope, the weak layer is cut with a snow saw from  
 508 its lower end continuing upslope. Possible fracture results are described in the inset. Here, we only  
 509 consider tests where the fracture went to the end of the column (End).



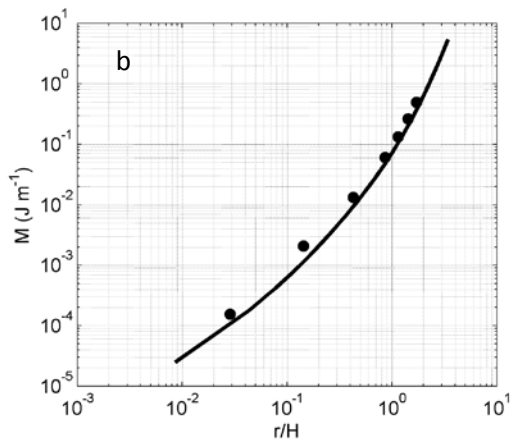
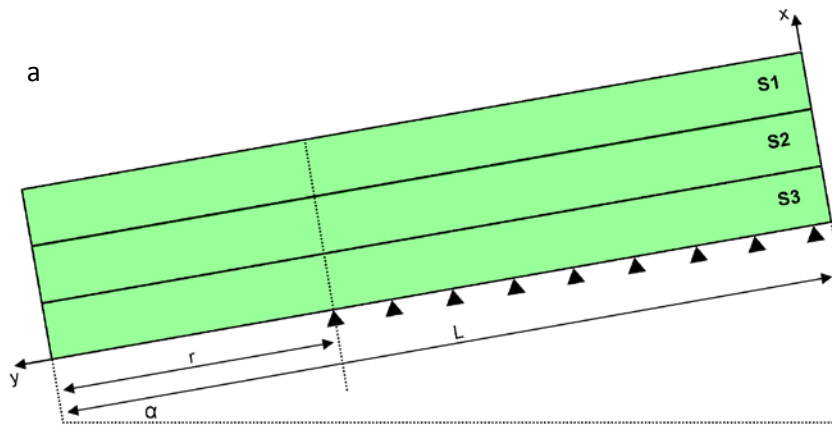
510 Figure 3: Penetration resistance (black) as measured with the SMP vs. snow depth. Slab layers (S1 to  
 511 S5) shaded in light green, weak layer (W) shaded in light red, basal layer (B) shaded in light orange.  
 512 50 mm of air signal cut off.



513 Figure 4: (a) FE model to simulate the maximum shear stress at the depth of the weak layer  
 514 consisting of three slab layers (green), the weak layer (red) and a basal layer below (orange) inclined  
 515 by the slope angle  $\alpha$ . Triangles indicate fixed nodes. The applied strip load  $P$  is illustrated by black  
 516 arrows pointing towards the snow surface. The axes of the coordinate system are indicated by  
 517 arrows. (b) Maximum shear stress from FE simulations (dots) and from the analytical solution (line)  
 518 for a uniform slab with density  $200 \text{ kg m}^{-3}$  and a slope angle of  $38^\circ$  versus slab thickness  $H$ .

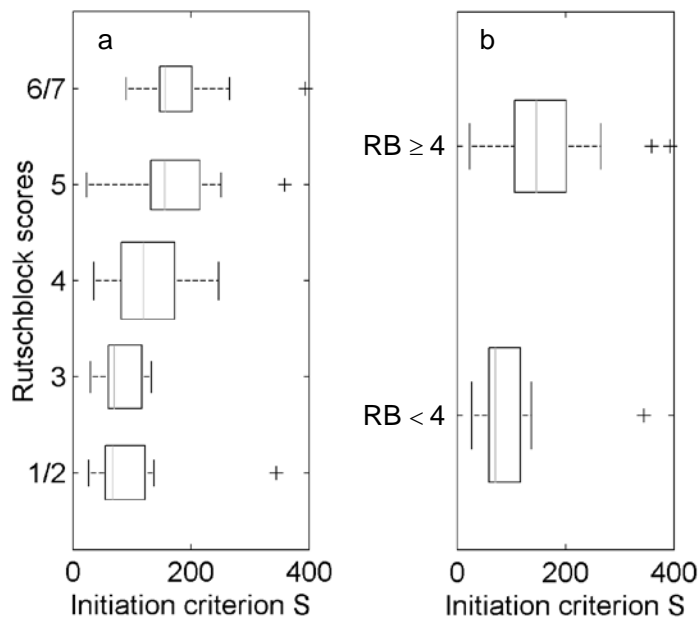


519 Figure 5: The polynomial's (Eq. 5) discriminant versus slab density for typical values of slab thickness  
 520 (colors); different line styles indicate flat terrain (dashed) and a slope inclined by  $\alpha = 38^\circ$  (solid lines).

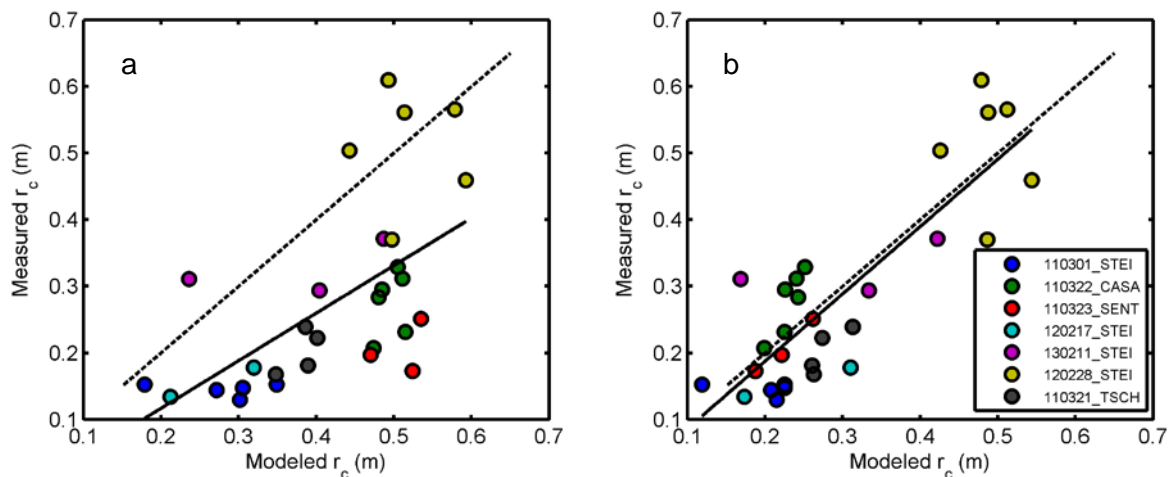


521 Figure 6: (a) The FE model to calculate the equivalent effective modulus contains as many slab layers  
 522 as necessary to reflect the stratigraphy found in the SMP signal. Triangles indicate fixed nodes. The  
 523 beam of length  $L$  is overhanging a crack of length  $r$  and is inclined by the slope angle  $\alpha$ . (b)  
 524 Mechanical energy  $M$  over the ratio of crack length and slab thickness ( $r/H$ ) modeled with FE (dots)  
 525 and calculated from the analytical solution (line) for a homogeneous slab with density  $200 \text{ kg m}^{-3}$  and  
 526 a slope angle of  $30^\circ$ .

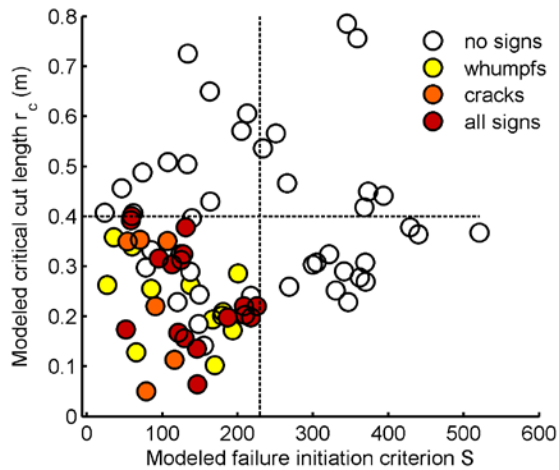




527 Figure 7: Modeled failure initiation criterion  $S$  (a) vs. RB score and (b) vs. RB stability classes: RB < 4  
 528 (N = 38) and RB  $\geq$  4 (N = 26). Boxes span the interquartile range from 1st to 3rd quartile with a  
 529 horizontal line showing the median (grey line). Widths of the boxes correspond to the number of  
 530 cases. Whiskers extend to the most extreme data points not considered outliers (crosses) within 1.5  
 531 times the interquartile range above the 3<sup>rd</sup> and below the 1<sup>st</sup> quartile.



532 Figure 8: Critical crack lengths  $r_c$  predicted from Eq. 7 are contrasted with critical crack lengths  
 533 measured in the field (N = 31). Experiments grouped by date and location with colors. Solid line  
 534 shows linear regression, dashed line indicates the 1:1 line. (a) Slab stratigraphy neglected (average  
 535 density, average effective modulus). (b) Density and effective modulus of each snow layer taken into  
 536 account by FE simulation.



537 Figure 9: Type and presence of signs of instability against failure initiation criterion  $S$  and critical crack  
 538 length  $r_c$ , both modeled, for datasets A and B, if reported ( $N = 77$ ). Colors indicate type of observed  
 539 signs of instability: whumpfs, shooting cracks with or without whumpfs (cracks) or all signs  
 540 (whumpfs, cracks and recent avalanches observed). Open circles indicate that no signs of instability  
 541 were reported explicitly (no signs). Dashed lines represent split values dividing the plot into four  
 542 quadrants as found with a classification tree.

# A process-based approach to estimate point snow instability

Benjamin Reuter, Jürg Schweizer, Alec van Herwijnen

WSL Institute for Snow and Avalanche Research SLF, Flüelastrasse 11, 7260 Davos Dorf, Switzerland

1 **Abstract:** Snow instability data provide information about the mechanical state of the snow cover  
2 and are essential for forecasting snow avalanches. So far, direct observations of instability (recent  
3 avalanches, shooting cracks or whumpf sounds) are complemented with field test such as the  
4 rutschblock test, since no measurement method for instability exists. We propose a new approach  
5 based on snow mechanical properties derived from the snow micro-penetrometer that takes into  
6 account the two essential processes during dry-snow avalanche release: failure initiation and crack  
7 propagation. To estimate the propensity of failure initiation we define a stress-based failure  
8 criterion, whereas the propensity of crack propagation is described by the critical cut length as  
9 obtained with a propagation saw test. The input parameters include layer thickness, snow density,  
10 effective elastic modulus, strength and specific fracture energy of the weak layer – all derived from  
11 the penetration-force signal acquired with the snow micro-penetrometer. Both instability measures  
12 were validated with independent field data and correlated well with results from field tests.  
13 Comparisons with observed signs of instability clearly indicated that a snowpack is only prone to  
14 avalanche if the two separate conditions for failure initiation and crack propagation are fulfilled. To  
15 our knowledge, this is the first time that an objective method for estimating snow instability has  
16 been proposed. The approach can either be used directly based on field measurements with the  
17 snow micro-penetrometer, or be implemented in numerical snow cover models. With an objective  
18 measure of instability at hand, the problem of spatial variations of instability and its causes can now  
19 be tackled.

## 20 1 Introduction

21 Snow slope stability describes the mechanical state of the snow cover on an inclined slope and is  
22 inversely related to the probability of avalanche release (McClung and Schaerer, 2006). For a given  
23 time, depth within the snowpack, and location on a slope, snow stability can be described as the  
24 balance between snow strength and stress termed stability index (Roch, 1966). This index has been  
25 widely used (e.g. Conway and Abrahamson, 1984; Perla et al., 1982) and refined by taking into  
26 account triggering by an additional load such as a skier (Föhn, 1987). Whereas, the skier stability  
27 index has been shown to be related to the probability of skier triggering (Jamieson, 1995), this critical  
28 stress approach does not take into account that slope failure requires crack propagation. While  
29 failure initiation may depend on stress only, the propagation of cracks requires deformation energy  
30 (Bazant and Planas, 1998). Furthermore, on a slope, strength and stress are spatially variable; these  
31 variations are fundamental to the fracture process (Schweizer et al., 2003). Around locally failed  
32 areas stress concentrations will form and drive crack propagation, and eventually cause catastrophic  
33 failure before the average material strength is reached. This observation has been termed knock-  
34 down effect (Fyffe and Zaiser, 2004) and partly explains why the stability index derived from  
35 measurements at or near natural slab avalanches often indicated stable conditions ([Perla, 1977](#)).

36 Not surprisingly, the link between point observations of snow stability and snow slope stability is not  
37 clear, yet (e.g. Bellaire and Schweizer, 2011). Scale issues due to different measurement scales, the  
38 so-called support and knowledge gaps between the processes involved at both scales have  
39 complicated bringing together point and slope scale snow instability results (Schweizer et al., 2008a).  
40 The point stability scale is not even well defined. Failure initiation refers to the collective failing of  
41 snow grains, or bonds between grains, on the scale of centimeters and the onset of a self-  
42 propagating crack in a weak snow layer called crack propagation. A common scale for both processes  
43 is the snowpack scale which spans about one square meter (Schweizer and Kronholm, 2007) which in  
44 the following we will refer to when we use the term point snow instability.

45 The stability index assumes a transition from stable to unstable when driving forces are no longer  
46 balanced by resisting forces. However, this approach is questionable, primarily since dry-snow slab  
47 avalanche release is the result of a series of fractures and snow properties are spatially variable. In a  
48 fracture mechanical view, to describe a material's resistance to crack propagation, flaw size and  
49 toughness need to be considered additionally to the stresses (Anderson, 1995). With the  
50 introduction of the propagation saw test (PST) (Gauthier and Jamieson, 2006; Sigrist and Schweizer,  
51 2007) all these properties can be obtained from field data. PST experiments to study propagating  
52 cracks have confirmed deformation of the slab to substantially contribute to the mechanical energy  
53 consumed by crack extension (van Herwijnen et al., 2010). Further, Gauthier and Jamieson (2008b)  
54 have shown that the critical crack length together with the fracture result are related to slope  
55 instability. In particular, cracks propagating to the end of the column after saw cut lengths less than  
56 50 % of the column length were clear indicators of high crack propagation propensity.

57 There is presently no objective measurement of snow instability. Instead, recent avalanches,  
58 whumpfs or shooting cracks are considered indicators of instability (Jamieson et al., 2009), but these  
59 observations are rare. In their absence the remaining option to gather field data on snow instability is  
60 snow instability testing (Schweizer and Jamieson, 2010). The rutschblock (RB) is a traditional snow  
61 stability test (Schweizer, 2002). The RB score was found indicative of the failure initiation propensity,  
62 the RB release type of the crack propagation propensity (Schweizer et al., 2008b). Whereas the RB  
63 release type only represents an ordinal rank, the propagation saw test (PST) gives a metric value, the  
64 critical cut length, which eases quantitative analysis. A combination of the results of both tests  
65 therefore seems appropriate for snow instability assessment.

66 Several studies focused on snow instability in the past, thereby either concentrating on failure  
67 initiation or crack propagation. Both, Bellaire et al. (2009) and Pielmeier and Marshall (2009) derived  
68 stability related parameters from measured snow micro-penetrometer resistance profiles. They  
69 found that weak layer strength and average slab density predicted with good accuracy stability  
70 classes estimated from RB tests.

71 Under the assumption of a uniform slab on a rigid substratum Heierli (2008) presented estimates of  
72 critical crack lengths obtained from recalculation of PST field experiments. Yet, averaging slab  
73 properties is a strong simplification and Schweizer (1993) pointed out the importance of slab  
74 properties for failure initiation. By means of linear elastic finite element (FE) simulations of typical  
75 snow profile types Habermann et al. (2008) found the stress at the depth of the weak layer to vary by  
76 a factor of two compared to a uniform slab. McClung (2009) suggested an alternative model to  
77 estimate the critical crack length by considering a finite fracture process zone.

78 Several numerical approaches focusing on avalanche release (for a summary see Podolskiy et al.,  
79 2013) have been made but only a few incorporate both fracture processes. Among the latest were  
80 Gaume et al. (2013) who presented a Mohr-Coulomb failure criterion based model taking into  
81 account variations of weak layer shear strength and stress redistribution by slab elasticity. Only  
82 lately, a possible refinement of the classical stability index by accounting for strength variations and  
83 their knock-down effect including a derivation of a critical crack length was presented (Gaume et al.,  
84 2014).

85 Predicting snow instability requires snow properties obtained either from field measurements or  
86 from snow cover modeling. In the field, the method of choice is the snow micro-penetrometer (SMP)  
87 (Schneebeli and Johnson, 1998) that allows deriving microstructural and micromechanical properties  
88 from the penetration force-distance signal (Johnson and Schneebeli, 1999). Marshall and Johnson  
89 (2009) showed that values of snow density, elastic modulus and strength derived from snow micro-  
90 penetrometer signals compared well with literature data. Interpreting the oscillation of the  
91 penetration force as a Poisson shot-noise process Löwe and van Herwijnen (2012) suggested a more  
92 robust method to extract the microstructural parameters. Their method was employed by Proksch et  
93 al. (2014) who developed a reliable parameterization of snow density applicable to a wide range of  
94 snow types. Reuter et al. (2013) showed that with the snow micro-penetrometer apart from snow  
95 density and effective modulus also the specific fracture energy of the weak layer can be derived.  
96 Comparing the results for mechanical properties obtained with snow micro-tomography (Schneebeli,  
97 2004) to those with particle tracking velocimetry of propagation saw tests (van Herwijnen et al.,  
98 2010) they substantiated the reliability of SMP-derived parameters.

99 Alternatively, snow cover models provide snow structural information allowing snow instability  
100 modeling (Durand et al., 1999; Lehning et al., 2004). However, snow mechanical properties are often  
101 not simulated independently, but parameterized on density only. Schweizer et al. (2006) refined the  
102 skier's stability index implemented in the snow cover model SNOWPACK and validated it with field  
103 observations. By first identifying the potential weakness in a simulated profile and then assessing its  
104 stability Monti et al. (2014) improved this approach to classify profiles into three classes of snow  
105 instability: poor, fair and good.

106 Given the fracture mechanical context of dry-snow slab avalanche release and the lack of an  
107 objective measure of instability, we propose that a description of instability should take into account  
108 the two essential processes in slab avalanche release, i.e. failure initiation and crack propagation,  
109 and be based on snow mechanical properties measured with the snow micro-penetrometer. Our goal  
110 is to provide an observer-independent methodology applicable to field measurements of snow  
111 stratigraphy. To this end we introduce a two-step calculation of a stability criterion and a critical  
112 crack length based on snow mechanical properties measured with the SMP. Then, we will validate  
113 the performance of our approach with field experiments of snow instability. Finally, we will show  
114 how classical snow instability observations may be interpreted in terms of failure initiation and crack  
115 propagation.

## 116 **2 Methods**

117 First, we present the experimental data, and then we describe how the mechanical field data  
118 acquired with the snow micro-penetrometer was analyzed, before we introduce the new approach  
119 to derive snow instability.

## 120 2.1 Field data

121 Two datasets of SMP measurements were exploited to test the performance of the failure initiation  
122 (A) and the crack propagation (B) part of our approach. Dataset A was originally presented by Bellaire  
123 et al. (2009). As meta data on snow instability was only available for a share of the data, 64 SMP  
124 measurements were kept for further analysis. They were all performed in close proximity (<0.5 m) to  
125 a RB test. The main results of a RB test, which is a point observation, are score and release type  
126 (Figure 1). We used the score for validating the failure initiation propensity (Schweizer and Jamieson,  
127 2010).

128 Dataset B consists of 31 SMP measurements which have been performed in a distance less than  
129 30 cm from the lower end of the column of propagation saw tests (PST) (Figure 2). Data were  
130 collected on seven different days. We filmed the fractures in the PSTs to precisely determine the  
131 onset of propagation by measuring the critical cut length in the pictures as a criterion of crack  
132 propagation.

133 Both datasets also include manually observed snow profiles including snow grain type and size and  
134 hand hardness index [for each manually identified layer](#). In addition, 77 out of the 95 field records in  
135 total contain information on either type or absence of signs of instability.

## 136 2.2 Snow micro-penetrometer

137 With the snow micro-penetrometer (SMP) a penetration resistance profile is recorded to a depth  
138 well below the weak layer at sub-millimeter resolution. Based on the detailed manually observed  
139 snow profile layers were defined from the corresponding sections of the signal, namely slab layers, a  
140 weak layer and a basal layer. As every layer is later represented in a finite element (FE) model and  
141 the resolution of the SMP is higher than the one needed for FE simulations, we deal with layers for  
142 the sake of shorter computation times. Figure 3 shows an example of a SMP signal with manually  
143 assigned snow layer boundaries.

144 Applying the shot-noise model by Löwe and van Herwijnen (2012) snow micro-structural parameters,  
145 namely the rupture force  $f$ , the deflection at rupture  $\delta$  and the structural element size  $L$  were  
146 calculated over a moving window  $w$  of 2.5 mm with 50% overlap and then averaged over the layer.  
147 Snow density was calculated as described in Proksch et al. (2015):

$$148 \rho = a_1 + a_2 \log(\tilde{F}) + a_3 L \log(\tilde{F}) + a_4 L \quad (1)$$

149 where  $a_i$  are coefficients,  $F$  is the penetration resistance and tilde denotes the median. The micro-  
150 mechanical effective modulus and strength were calculated according to Johnson and Schneebeli  
151 (1999):

$$152 E = \frac{f}{\delta L} \quad (2)$$

153 and

$$154 \sigma = \frac{f}{L^2} \quad (3)$$

155 The specific fracture energy of the weak layer (WL) was calculated as the minimum of the  
156 penetration resistance integrated across the window size  $w$  within the weak layer (Reuter et al.,  
157 2013):

158  $w_f = \min_{WL} \int_{-\frac{w}{2}}^{+\frac{w}{2}} F dz .$  (4)

159 The penetration depth PS was derived by integrating from the snow surface over the penetration  
 160 resistance F to a threshold absorbed energy  $e_a = 0.0036$  J, which had been determined by comparison  
 161 of SMP profiles with concurrently observed penetration depth (Schweizer and Reuter, 2015):

162  $e_a = \int_0^{PS} F(z) dz.$  (5)

163 **2.3 Modeling**

164 In the following the modeling approach to calculate estimates of the failure initiation and the crack  
 165 propagation propensity of a certain slab-weak layer combination is described and validated. The  
 166 mechanical properties required as input are obtained from the SMP signal as described above.

167 *2.3.1 Failure initiation*

168 A strength-over-stress criterion *S* describes the propensity of the weak layer to fail in the case of an  
 169 additional load:

170  $S = \frac{\sigma_{WL}}{\Delta\tau},$  (6)

171 with  $\sigma_{WL}$  being the strength of the weak layer and  $\Delta\tau$  being the maximum additional shear stress at  
 172 the depth of the weak layer due to skier loading. The strength of the weak layer is approximated by  
 173 the micro-mechanical strength derived from the snow micro-penetrometer signal in the weak layer,  
 174 i.e. we cannot use the slope-parallel shear strength because the SMP is an indentation test  
 175 measuring an effective strength resulting from the mixed-mode breaking of bonds at the tip. The  
 176 maximum shear stress at the depth of the weak layer was modeled with the 2D linear elastic finite  
 177 element (FE) model originally designed by Habermann et al. (2008) to calculate the shear stress at  
 178 the depth of the weak layer below a layered slab due to the weight of a skier. *S* may be interpreted  
 179 as an indicator of failure initiation with low (high) values being associated with high (low) likelihood  
 180 of initiating a failure. Note, the stability criterion *S* is not expected to yield typical values of the skier's  
 181 stability index (< 1 for 'unstable', > 1.5 for 'stable') (Jamieson and Johnston, 1998). One reason is that  
 182 SMP-derived strength values are about two orders of magnitude larger than values of shear strength  
 183 reported in literature (Marshall and Johnson, 2009) as the SMP measurement is an indentation test.

184 The 2D FE model by Habermann et al. (2008) has been adopted to include all relevant slab layers –  
 185 usually about 5 to 10 layers. The geometry of the model (Figure 4a) was chosen such that the length  
 186 of the modeled section of the snowpack (10 m) is at least one order of magnitude larger than the  
 187 average depth of the weak layer to keep boundary effects small. The model consists of multiple  
 188 layers including slab and basal layers as well as an embedded weak layer corresponding to the  
 189 layering identified in the SMP signal. The layers are inclined by the slope angle  $\alpha$ . Nodes at the lower  
 190 end (on the right of Figure 4a) and at the snow soil interface were fixed in both coordinate directions.

191 The model domain was divided into two-dimensional, quadrilateral plane strain elements having  
 192 eight nodes each. The mesh consisted of 75 nodes in the horizontal and 100 nodes in the vertical per  
 193 meter. The model has been implemented in ANSYS workbench to calculate the maximum shear  
 194 stress within the weak layer. We assumed plane strain as stresses in the direction normal to the x-y

195 plane are smaller than within and linear elastic behavior as the loading rate is high considering skier  
 196 loading. The skier load was modeled as a static strip load  $\underline{P}$  of 780 N spread over a width  $a$  of 0.2 m.  
 197 To account for skier penetration we assumed the layers within the penetration depth to be  
 198 compacted to a density of  $300 \text{ kg m}^{-3}$  with a corresponding elastic modulus of 16 MPa according to  
 199 Scapozza (2004), i.e. density and thickness of slab layers were adjusted. All snow layers in the FE  
 200 model were assigned thickness, density and effective modulus values as derived from the SMP signal.  
 201 A fixed value of the Poisson's ratio was chosen ( $\nu = 0.25$ ). From the modeled linear elastic behavior  
 202 the maximum shear stress within the weak layer was computed yielding  $\Delta\tau$  of Eq. 6, i.e. not  
 203 considering the stress due to the weight of the slab.

204 The FE model was tested to reproduce the analytical solution of McClung and Schweizer (1999) for  
 205 the shear stress for a strip load on a finite area  $\tau(\theta, H)$  where  $\theta$  and  $H$  are two-dimensional polar  
 206 coordinates. To do so, the maximum shear stress at a certain depth  $H$  was determined by varying  $\theta$ .  
 207 The FE model was run with a Poisson's ratio of  $\nu = 0.49$ , as the analytical solution assumes an  
 208 incompressible half space. The slab was not stratified, but uniform having a density of  $200 \text{ kg m}^{-3}$ .  
 209 Hence, the solution is independent of the elastic modulus. The simulation results for different slab  
 210 thickness  $H$  are presented in Figure 4b together with the analytical solution. The FE model  
 211 reproduced the maximum shear stress as obtained with the analytical solution very well ( $R^2 = 0.94$ ,  
 212 regression slope  $m = 1.2$ ) especially for slab depth larger than the width of skier load (0.2 m).

### 213 2.3.2 Crack propagation

214 In order to estimate the crack propagation propensity the critical crack length as measured in a PST  
 215 experiment was calculated for a weak layer embedded by a layered slab and a basal layer.

216 A theoretical expression (Eq. 7) linking the fracture energy of the weak layer, the elastic modulus of  
 217 the slab and the critical crack length for a self-propagating crack is obtained by replacing the  
 218 mechanical energy in Griffith's criterion with the total energy of the slab weak layer system found by  
 219 (Heierli, 2008) and was presented in detail by Schweizer et al. (2011). The formulation of the total  
 220 mechanical energy of the slab-weak layer system has been proven to describe the released  
 221 mechanical energy of the slab in a PST reasonably well (van Herwijnen et al., 2010).

$$222 \quad w_f(E, r_c) = \frac{H}{2E} \left[ w_0 + w_1 \frac{r_c}{H} + w_2 \left( \frac{r_c}{H} \right)^2 + w_3 \left( \frac{r_c}{H} \right)^3 + w_4 \left( \frac{r_c}{H} \right)^4 \right], \quad (7)$$

223 with

$$w_0 = \frac{3\eta^2}{4} \tau^2,$$

$$w_1 = \left( \pi\gamma + \frac{3\eta}{2} \right) \tau^2 + 3\eta^2 \tau\sigma + \pi\gamma\sigma^2,$$

$$w_2 = \tau^2 + \frac{9\eta}{2} \tau\sigma + 3\eta^2 \sigma^2,$$

$$w_3 = 3\eta\sigma^2,$$

$$w_4 = 3\sigma^2,$$

224 and  $\tau = -\rho g H \sin(\alpha)$  the shear stress,  $\sigma = -\rho g H \cos(\alpha)$  the normal stress,  $\gamma = 1$  the elastic mismatch  
 225 parameter,  $\eta = \sqrt{4(1 + \nu)/5}$  and  $\nu = 0.25$ . Provided the elastic modulus  $E$ , the density  $\rho$  and the  
 226 thickness of the slab  $H$ , the fracture energy of the weak layer  $w_f$ , and the slope angle  $\alpha$  are known,  
 227 the calculation of the critical crack length  $r_c$  reduces to finding the roots of Eq. 7. This fourth degree



228 polynomial of  $r_c$  has real, ever positive coefficients. Figure 5 illustrates the dependence of the  
 229 polynomial's discriminant on slab thickness and density, which is the case if a dependence of the  
 230 elastic modulus on density is assumed. As the polynomial's discriminant does not change sign for  
 231 typical values of density (and the elastic modulus), solutions consist of a pair of complex conjugated  
 232 and two real roots. A physically meaningful solution of  $r_c$  is obtained, if the complex roots and the  
 233 one with an unexpected sign are discarded.

234 To relax the assumption of a uniform, i.e. not stratified, slab a FE model was designed to determine  
 235 the equivalent bulk modulus  $E'$  of a stratified slab (Figure 6a). The model performed a stepwise  
 236 calculation of the mechanical strain energy  $M$  of a stratified slab due to bending over an increasing  
 237 crack of length  $r$ . In order to recover an equivalent bulk modulus  $E'$ , in a next step the pairs of  
 238 mechanical energy and crack length ( $M$ ,  $r$ ) were fitted with a theoretical expression of the total  
 239 mechanical energy of the slab  $M$  (Heierli, 2008):

$$240 \quad M(E', r) = -\frac{\pi\gamma r^2}{4E'}(\tau^2 + \sigma^2) - \frac{r^3}{6E'H}[\lambda_{\tau\tau}\tau^2 + \lambda_{\sigma\tau}\tau\sigma + \lambda_{\sigma\sigma}\sigma^2], \quad (8)$$

241 with

$$242 \quad \lambda_{\tau\tau} = 1 + \frac{9}{4}\eta\left(\frac{r}{H}\right)^{-1} + \frac{9}{4}\eta^2\left(\frac{r}{H}\right)^{-2},$$

$$243 \quad \lambda_{\tau\sigma} = \frac{9}{2}\eta + \frac{9}{2}\eta^2\left(\frac{r}{H}\right)^{-1},$$

$$244 \quad \lambda_{\sigma\sigma} = 3\eta^2 + \frac{9}{4}\eta\frac{r}{H} + \frac{9}{5}\left(\frac{r}{H}\right)^2.$$

245 The FE model consists of stratified layers, which were assigned SMP-derived values of density,  
 246 effective modulus and thickness (Figure 6a). The Poisson's ratio was kept constant ( $\nu = 0.25$ ). Due to  
 247 its geometry (only considering slab layers) and boundary conditions (rigid support along the ligament  
 248 length ( $L-r$ )) the FE model only considers the behavior of the slab layers as described with the  
 249 formulation of the total mechanical energy of the slab-weak layer system, neglecting deformation in  
 250 the weak or basal layers. In our model, the deflecting beam never got in touch with the basal layer,  
 251 which, however, may be the case in field experiments, in particular with soft slabs. The FE model  
 252 reproduced the theoretical formulation very well ( $R^2 = 0.85$ ), especially for crack lengths  $r$  greater or  
 253 equal the thickness of the overlying slab  $H$  (Figure 6b). With the bulk equivalent modulus  $E'$ , we find  
 254 the exact solution of Eq. 7 and receive the critical crack length  $r_c$  for the specific slab-weak layer  
 255 combination.

## 256 3 Results

257 In the following both model parts predicting the propensity of the snowpack to failure initiation and  
 258 crack propagation are evaluated with the two independent data sets (A and B).

### 259 3.1 Failure initiation

260 For each of the 66 SMP profiles with corresponding RB test (dataset A) the failure initiation criterion  
 261  $S$  was calculated. SMP-derived density, effective modulus, strength and layer thickness were used to  
 262 drive the FE model. For the comparison with the RB score we grouped scores 1 and 2 as well as 6 and  
 263 7 because scores 1 and 7 were observed infrequently. The criterion  $S$  increased with increasing RB  
 264 score (Figure 7a). If for a given  $S$  there was no overlap of the boxes, the predictive power of  $S$  would

265 obviously be very good. Although this is not the case, the medians of the failure initiation criterion  
266 (indicated by gray lines) per RB score increased monotonically with increasing RB scores. This  
267 monotonic increase is reflected in a high Spearman rank correlation coefficient ( $r_s > 0.9$ ). If results are  
268 grouped by scores in two stability classes of  $RB < 4$  and  $RB \geq 4$ , a threshold previously found to  
269 separate lower and higher stability (e.g. Schweizer and Jamieson, 2003), the criterion  $S$  discriminated  
270 well between the two classes (Wilcoxon rank sum test, level of significance  $p = 0.01$ ) with a  
271 classification tree splitting value of  $S = 133$ .

### 272 3.2 Crack propagation

273 All 31 SMP signals from dataset B were analyzed and the critical cut length  $r_c$  was calculated from  
274 Eq. 7 with SMP-derived mechanical properties being density, effective modulus, specific fracture  
275 energy and layer thickness. In Figure 8 the results are contrasted with the critical crack lengths  
276 measured in the field in the PST experiments adjacent to the SMP measurements. On the left  
277 (Figure 8a) model results are shown for the case of a uniform slab, i.e. density and effective modulus  
278 were averaged to show the effect of neglecting the stratigraphy of the slab. Modeled values  
279 overestimated the critical cut length yielding a rather fair Pearson correlation coefficient of  $r_p = 0.58$   
280 and a coefficient of determination of  $R^2 = 0.29$ . Only for a few experiments modeled and observed  
281 crack lengths were similar indicating that assuming a uniform slab is not a good approximation. In  
282 fact, Figure 8b shows that the agreement between model results and observations improved if the  
283 stratification of the slab was taken into account. All identified slab layers were assigned the  
284 corresponding density and effective modulus obtained from SMP signal processing and input in the  
285 FE model to determine the bulk effective modulus of the slab. The modeled values of critical crack  
286 length were clearly related to the measured values ( $r_p = 0.83$ ) as indicated by the collapse of the  
287 linear regression on the 1:1 line (Figure 8b). The regression slope was well-defined ( $p < 0.01$ ) with  
288 some scatter ( $R^2 = 0.50$ ) indicating the uncertainty involved with the presented approach. The critical  
289 crack length was predicted with a root mean squared error of 2 cm, a mean absolute error of 7 cm  
290 and a mean absolute percentage error of 9%.

### 291 3.3 Validation with signs of instability

292 Model results were further compared with independent field observations of signs of instability such  
293 as whumpfs, shooting cracks and recent avalanches. Both datasets (A and B) included records of such  
294 field observations which we grouped in three categories: whumpfs, shooting cracks with or without  
295 whumpfs ('cracks') or 'all signs' (whumpfs, cracks and recent avalanches), i.e. fresh avalanches were  
296 only observed simultaneously with whumpfs and cracks (Figure 9). To jointly relate our modeled  
297 estimates of instability to the observations of instability we contrasted the propensity to crack  
298 propagation, i.e. modeled critical crack length, and failure initiation, i.e. initiation criterion  $S$ , in  
299 Figure 9. Signs of instability were primarily present in the lower left of Figure 9, i.e. for low values of  
300 the failure initiation criterion and the critical crack length. Vice versa no signs of instability were  
301 reported if both criteria yielded high values (upper right). This finding suggests that both criteria, the  
302 one for failure initiation and the one for crack propagation, are linked to snow instability. A  
303 classification tree with the two independent variables  $S$  and  $r_c$  yielded splits of  $S = 234$  and  $r_c = 0.41$  m  
304 which separate between the cases with and without concurrently observed signs of instability (Figure  
305 9). These thresholds divide the plot into four quadrants. In the lower left quadrant all 35 cases with

306 signs of instability as well as ten cases without signs of instability were found. Our split value ( $S=234$ )  
307 for the initiation criterion  $S$  is very similar to the one found by Schweizer and Reuter (2015) who  
308 reported a value of 212. In regard to the modeled critical crack length, Gauthier and Jamieson  
309 (2008a) suggested a value of <50% of the column length which in their study corresponded to 50 cm.  
310 Assuming crack propagation to be likely (two lower quadrants) or failure initiation to be easy (two  
311 left quadrants) does not distinguish sharply between signs of instability present or absent. However,  
312 if both criteria had low values unstable snow conditions were observed (lower left quadrant).

## 313 **4 Discussion**

314 In our present understanding avalanche release is seen as a sequence of fractures. To capture the  
315 two most important steps preceding the detachment of a snow slab we addressed the stress at the  
316 depth of a potential weakness with the failure initiation criterion  $S$  and the critical crack size for self-  
317 propagation with the critical crack length  $r_c$ . We presented a model approach to derive both  
318 quantities from snow micro-penetrometer signals which is a fast method to acquire information on  
319 mechanical properties in the field.

320 Assessing the performance of the model approach with two different field tests (RB and PST) yielded  
321 plausible results. However, the main source of uncertainty is related to the mechanical properties  
322 needed as input for the model. Snow density, effective modulus and specific fracture energy were all  
323 determined from SMP measurements. Uncertainties related to the determination of these  
324 mechanical properties have recently been addressed by Proksch et al. (2015) and Reuter et al. (2013)  
325 and lie within 10-20% for density and fracture energy. Other SMP error sources are known and so  
326 erroneous signals were identified and discarded. Some errors were user-related such as mechanical  
327 disturbances. Other unavoidable errors such as signal drift due to strong temperature changes in the  
328 snowpack or stick slip of the rod at high snow densities were rare.

329 The SMP-derived failure initiation criterion  $S$  performed well based on the evaluation with  
330 rutschblock tests, yielding a better correlation than the one lately observed by Schweizer and Reuter  
331 (2014) using the compression test. They concluded that the dimensions of the compression test and  
332 the type of loading are not ideal for modeling purposes. While the RB test includes six different  
333 loading steps, the load is only increased twice in a compression test, but numerous taps are  
334 performed within the same loading range. The loading of the RB and consequently the stress exerted  
335 on the weak layer increases monotonically with the score (score four and five have the same load).  
336 This is reflected in the fair discrimination of RB scores four and five with the failure initiation  
337 criterion  $S$ . Furthermore, RB loading steps are ordinal numbers, i.e. they can be ranked, but they do  
338 not follow a known relation with stability. Hence, the stress in the weak layer increases stepwise in  
339 the experiment, whereas the modeled stability is continuous. The boxplots in Figure 7 group  
340 modeled values of failure initiation ( $S$ ) with rutschblock classes. The monotonic increase of the  
341 medians suggests that the criterion  $S$  reflects the propensity of failure initiation in a weak layer below  
342 a layered slab. Correlations of the rutschblock release type were neither significant with the initiation  
343 criterion  $S$  ( $r_s = 0.11$ ,  $p = 0.39$ ), nor with the modeled critical cut length ( $r_s = 0.04$ ,  $p = 0.76$ ).

344 The critical cut length was modeled with an accuracy of a few centimeters (RMSE of 2 cm). It was  
345 shown that the slab layering played an important role in the process of crack propagation. Only with  
346 the introduction of the bulk effective modulus imitating the bending behavior of a layered slab

347 measured critical cut lengths were reproduced with good accuracy (Figure 8). Until now research on  
348 snow instability had mainly focused on weak layer or average slab properties (Bellaire et al., 2009;  
349 Pielmeier and Marshall, 2009). Alternatively, the critical value of the crack length could have been  
350 determined by stepwise increasing the crack length in an FE model until the critical energy release  
351 rate reaches the specific fracture energy of the weak layer. This approach, [comparable to the one by](#)  
352 [Mahajan and Joshi \(2008\)](#), however, was not followed due to its high computational expenses, as  
353 repeated meshing for every single iteration step would be costly.

354 The introduced FE models assumed linear elastic behavior and were confined to two dimensions.  
355 These assumptions are in contrast with our knowledge that snow is a porous medium consisting of a  
356 non-isotropic ice/air matrix, exhibiting plastic, elastic and viscous behavior at the macro scale.  
357 However, as loading rates in RB tests and PSTs are high, linear elastic assumptions are justified – for  
358 the rutschblock test at least at a certain depth below the snow surface. Two dimensional modeling  
359 seems sufficient, as three dimensional modeling is not advantageous due to the lack of experimental  
360 orthotropic material properties at this point of time.

## 361 **5 Conclusions**

362 We have developed a novel approach to determine quantitative estimates of both, the failure  
363 initiation and crack propagation propensity of the snowpack based on mechanical properties derived  
364 from objective snow micro-penetrometer measurements. Based on the current understanding of  
365 dry-snow slab avalanche release it includes the mechanical properties of all relevant layers  
366 embedding the weak layer to make predictions on the propensity of initiating a failure and spreading  
367 the crack in a weak layer within the snowpack. The presented approach is process-based, observer-  
368 independent and relies on measurements of mechanical properties.

369 The performance of the two novel measures of instability has been assessed in comparisons with two  
370 different datasets of field tests (rutschblock and propagation saw test). Both measures of instability,  
371 the stress criterion  $S$  as well as the critical crack length  $r_c$  were well correlated with the results of field  
372 tests. In addition, the importance of slab layering especially with respect to crack propagation has  
373 been shown. The comparison of our modeled estimates of snow instability with field observations of  
374 signs of instability clearly indicated that a snowpack is unstable only in case of high failure initiation  
375 as well as high crack propagation propensity. Whereas we anticipated this finding, i.e. that both  
376 conditions have to be fulfilled, we are not aware, [to the best of our knowledge](#), that it has been  
377 demonstrated before.

378 Recent field studies have frequently focused on identifying spatial variations of snow instability and  
379 its drivers which requires an objective measure of instability – which was so far lacking. With the  
380 observer-independent method we presented taking into account both processes, failure initiation  
381 and crack propagation, it will become possible to resolve causes of spatial snow instability variations.  
382 With respect to operational application in the context of avalanche forecasting our approach can be  
383 employed directly based on field measurements, provided a robust and reliable snow micro-  
384 penetrometer is at hand which in addition allows remote data transfer, or be implemented in  
385 numerical snow cover models.

386 **Acknowledgements**

387 B.R. has been supported by a grant of the Swiss National Science Foundation (200021\_144392). We  
388 thank numerous colleagues from SLF for help with the field work. [We are grateful for the](#)  
389 [constructive review comments by E. Podolskiy and B. Jamieson.](#)

390 **References**

- 391 Anderson, T. L.: Fracture mechanics: fundamentals and applications, CRC Press, Boca Raton, U.S.A.,  
392 1995.
- 393 Bazant, Z. P. and Planas, J.: Fracture and size effect in concrete and other quasibrittle materials, CRC  
394 Press, Boca Raton, U.S.A., 1998.
- 395 Bellaire, S., Pielmeier, C., Schneebeli, M., and Schweizer, J.: Stability algorithm for snow micro-  
396 penetrometer measurements, *J. Glaciol.*, 55, 805-813, 2009.
- 397 Bellaire, S. and Schweizer, J.: Measuring spatial variations of weak layer and slab properties with  
398 regard to snow slope stability, *Cold Reg. Sci. Technol.*, 65, 234-241, 2011.
- 399 Conway, H. and Abrahamson, J.: Snow stability index, *J. Glaciol.*, 30, 321-327, 1984.
- 400 Durand, Y., Giraud, G., Brun, E., Mérindol, L., and Martin, E.: A computer-based system simulating  
401 snowpack structures as a tool for regional avalanche forecasting, *J. Glaciol.*, 45, 469-484, 1999.
- 402 Föhn, P. M. B.: The stability index and various triggering mechanisms, in: Symposium at Davos 1986  
403 – Avalanche Formation, Movement and Effects, IAHS Publ. 162, edited by: Salm, B. and Gubler,  
404 H., International Association of Hydrological Sciences, Wallingford, Oxfordshire, UK, 1987, 195-  
405 214.
- 406 Fyffe, B. and Zaiser, M.: The effects of snow variability on slab avalanche release, *Cold Reg. Sci.*  
407 *Technol.*, 40, 229-242, 2004.
- 408 Gaume, J., Chambon, G., Eckert, N., and Naaim, M.: Influence of weak-layer heterogeneity on snow  
409 slab avalanche release: application to the evaluation of avalanche release depths, *J. Glaciol.*,  
410 59, 423-437, 2013.
- 411 Gaume, J., Schweizer, J., van Herwijnen, A., Chambon, G., Reuter, B., Eckert, N., and Naaim, M.:  
412 Evaluation of slope stability with respect to snowpack spatial variability, *J. Geophys. Res.*, 2014.  
413 doi: 10.1002/2014JF00319, 2014.
- 414 Gauthier, D. and Jamieson, B.: Evaluation of a prototype field test for fracture and failure  
415 propagation propensity in weak snowpack layers, *Cold Reg. Sci. Technol.*, 51, 87-97, 2008a.
- 416 Gauthier, D. and Jamieson, B.: Fracture propagation propensity in relation to snow slab avalanche  
417 release: Validating the Propagation Saw Test, *Geophys. Res. Lett.*, 35, L13501, 2008b.
- 418 Gauthier, D. and Jamieson, J. B.: Towards a field test for fracture propagation propensity in weak  
419 snowpack layers, *J. Glaciol.*, 52, 164-168, 2006.
- 420 Habermann, M., Schweizer, J., and Jamieson, J. B.: Influence of snowpack layering on human-  
421 triggered snow slab avalanche release, *Cold Reg. Sci. Technol.*, 54, 176-182, 2008.
- 422 Heierli, J.: Anticrack model for slab avalanche release, Ph.D. Ph.D., University of Karlsruhe, Karlsruhe,  
423 Germany, 102 pp., 2008.
- 424 Jamieson, B., Haegeli, P., and Schweizer, J.: Field observations for estimating the local avalanche  
425 danger in the Columbia Mountains of Canada, *Cold Reg. Sci. Technol.*, 58, 84-91, 2009.
- 426 Jamieson, J. B.: Avalanche prediction for persistent snow slabs, 1995. Ph.D., Department of Civil  
427 Engineering, University of Calgary, Calgary AB, Canada, 258 pp., 1995.
- 428 Jamieson, J. B. and Johnston, C. D.: Refinements to the stability index for skier-triggered dry slab  
429 avalanches, *Ann. Glaciol.*, 26, 296-302, 1998.

430 Johnson, J. B. and Schneebeli, M.: Characterizing the microstructural and micromechanical properties  
431 of snow, *Cold Reg. Sci. Technol.*, 30, 91-100, 1999.

432 Lehning, M., Fierz, C., Brown, R. L., and Jamieson, J. B.: Modeling instability for the snow cover model  
433 SNOWPACK, *Ann. Glaciol.*, 38, 331-338, 2004.

434 Löwe, H. and van Herwijnen, A.: A Poisson shot noise model for micro-penetration of snow, *Cold Reg.*  
435 *Sci. Technol.*, 70, 62-70, 2012.

436 [Mahajan, P. and Joshi, S.K.: Modeling of interfacial crack velocities in snow, \*Cold Reg. Sci. Technol.\*,  
437 \*51\(2-3\)\*, 98-111, 2008.](#)

438 Marshall, H.-P. and Johnson, J. B.: Accurate inversion of high-resolution snow penetrometer signals  
439 for microstructural and micromechanical properties, *J. Geophys. Res.*, 114, F04016, 2009.

440 [McClung, D. M.: Dry snow slab quasi-brittle fracture initiation and verification from field tests, \*J.\*  
441 \*Geophys. Res.\*, 114, F01022, doi:10.1029/2007JF000913, 2009.](#)

442 McClung, D. M. and Schaerer, P.: *The Avalanche Handbook*, The Mountaineers Books, Seattle WA,  
443 U.S.A., 2006.

444 McClung, D. M. and Schweizer, J.: Skier triggering, snow temperatures and the stability index for dry  
445 slab avalanche initiation, *J. Glaciol.*, 45, 190-200, 1999.

446 Monti, F., Schweizer, J., and Gaume, J.: Deriving snow stability information from simulated snow  
447 cover stratigraphy, *Proceedings ISSW 2014. International Snow Science Workshop, Banff,*  
448 *Alberta, Canada, 29 September - 3 October 2014*, 465-469, 2014.

449 [Perla, R.: Slab avalanche measurements, \*Can. Geotech. J.\*, 14\(2\), 206-213, 1977.](#)

450 Perla, R., Beck, T. M. H., and Cheng, T. T.: The shear strength index of alpine snow, *Cold Reg. Sci.*  
451 *Technol.*, 6, 11-20, 1982.

452 Pielmeier, C. and Marshall, H.-P.: Rutschblock-scale snowpack stability derived from multiple quality-  
453 controlled SnowMicroPen measurements, *Cold Reg. Sci. Technol.*, 59, 178-184, 2009.

454 Podolskiy, E. A., Chambon, G., Naaim, M., and Gaume, J.: A review of finite-element modelling in  
455 snow mechanics, *J. Glaciol.*, 59, 1189-1201, 2013.

456 Proksch, M., Löwe, H., and Schneebeli, M.: Density, specific surface area and correlation length of  
457 snow measured by high-resolution penetrometry, *J. Geophys. Res.*, 120, doi:  
458 [10.1002/2014JF003266](#), 2015.

459 Reuter, B., Proksch, M., Loewe, H., van Herwijnen, A., and Schweizer, J.: On how to measure snow  
460 mechanical properties relevant to slab avalanche release, *Proceedings ISSW 2013.*  
461 *International Snow Science Workshop, Grenoble, France, 7-11 October 2013, 7-11, 2013.*

462 Reuter, B. and Schweizer, J.: The effect of surface warming on slab stiffness and the fracture behavior  
463 of snow, *Cold Reg. Sci. Technol.*, 83-84, 30-36, 2012.

464 Roch, A.: Les déclenchements d'avalanches. In: *Symposium at Davos 1965 - Scientific Aspects of*  
465 *Snow and Ice Avalanches*, IAHS Publication, 69, Int. Assoc. Hydrol. Sci., Wallingford, U.K., 1966.

466 Scapozza, C.: *Entwicklung eines dichte- und temperaturabhängigen Stoffgesetzes zur Beschreibung*  
467 *des visko-elastischen Verhaltens von Schnee*, Ph.D. thesis, Institut für Geotechnik, ETH Zurich,  
468 Zurich, Switzerland, 250 pp., 2004.

469 Schneebeli, M.: Numerical simulation of elastic stress in the microstructure of snow, *Ann. Glaciol.*, 38,  
470 339-342, 2004.

471 Schneebeli, M. and Johnson, J. B.: A constant-speed penetrometer for high-resolution snow  
472 stratigraphy, *Ann. Glaciol.*, 26, 107-111, 1998.

473 Schweizer, J.: The influence of the layered character of snow cover on the triggering of slab  
474 avalanches, *Ann. Glaciol.*, 18, 193-198, 1993.

475 Schweizer, J.: *The Rutschblock test - Procedure and application in Switzerland*, *The Avalanche*  
476 *Review*, 20, 1,14-15, 2002.



477 Schweizer, J. and Jamieson, J. B.: Snowpack properties for snow profile analysis, Cold Reg. Sci.  
478 Technol., 37, 233-241, 2003.

479 Schweizer, J. and Jamieson, J. B.: Snowpack tests for assessing snow-slope instability, Ann. Glaciol.,  
480 51, 187-194, 2010.

481 Schweizer, J. and Kronholm, K.: Snow cover spatial variability at multiple scales: Characteristics of a  
482 layer of buried surface hoar, Cold Reg. Sci. Technol., 47, 207-223, 2007.

483 Schweizer, J. and Reuter, B.: [A new index combining weak layer and slab properties for snow](#)  
484 [instability](#), Nat. Hazards Earth Syst. Sci., [15](#), 109-118, 2015.

485 Schweizer, J., Bellaire, S., Fierz, C., Lehning, M., and Pielmeier, C.: Evaluating and improving the  
486 stability predictions of the snow cover model SNOWPACK, Cold Reg. Sci. Technol., 46, 52-59,  
487 2006.

488 Schweizer, J., Jamieson, J. B., and Schneebeli, M.: Snow avalanche formation, Rev. Geophys., 41,  
489 1016, 2003.

490 Schweizer, J., Kronholm, K., Jamieson, J. B., and Birkeland, K. W.: Review of spatial variability of  
491 snowpack properties and its importance for avalanche formation, Cold Reg. Sci. Technol., 51,  
492 253-272, 2008a.

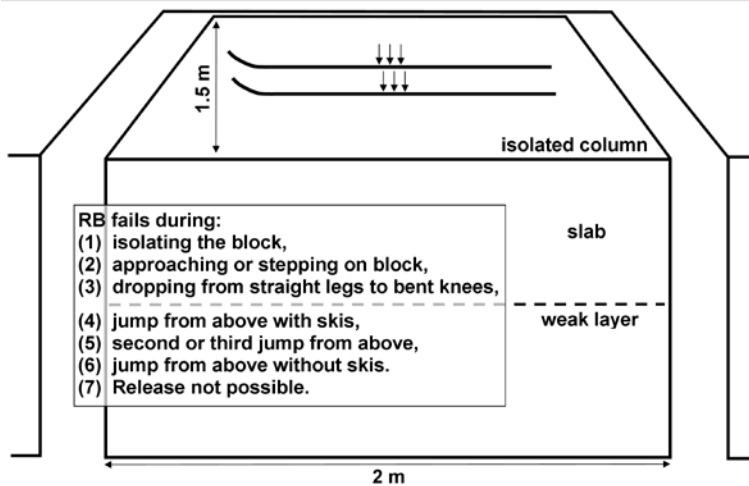
493 Schweizer, J., McCammon, I., and Jamieson, J. B.: Snowpack observations and fracture concepts for  
494 skier-triggering of dry-snow slab avalanches, Cold Reg. Sci. Technol., 51, 112-121, 2008b.

495 Schweizer, J., van Herwijnen, A., and Reuter, B.: Measurements of weak layer fracture energy, Cold  
496 Reg. Sci. Technol., 69, 139-144, 2011.

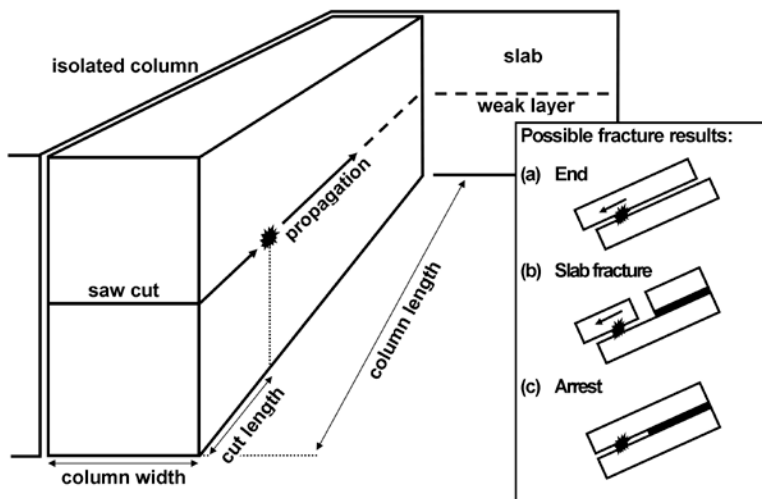
497 Sigrist, C. and Schweizer, J.: Critical energy release rates of weak snowpack layers determined in field  
498 experiments, Geophys. Res. Lett., 34, L03502, doi:03510.01029/02006GL028576, 2007.

499 van Herwijnen, A., Schweizer, J., and Heierli, J.: Measurement of the deformation field associated  
500 with fracture propagation in weak snowpack layers, J. Geophys. Res., 115, F03042,  
501 doi:03010.01029/02009JF001515, 2010.

Figure Captions and Figures

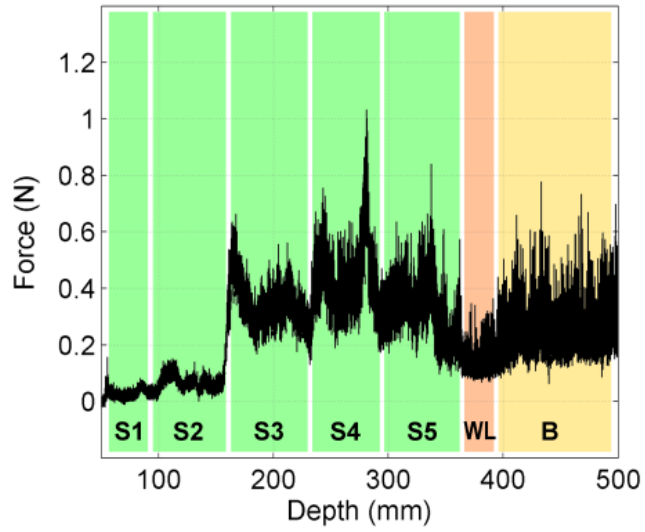


502 Figure 1: Sketch presenting the rutschblock (RB) test as it is seen looking upslope: After isolating a  
 503 block of snow 2 m wide and 1.5 m upslope it is loaded progressively by a skier. The loading steps and  
 504 scores are described in the inset. The release type was not considered here.

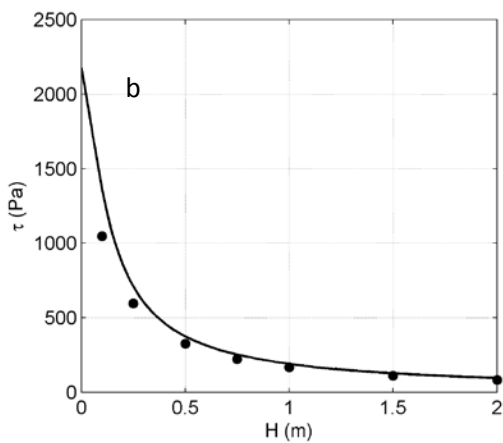
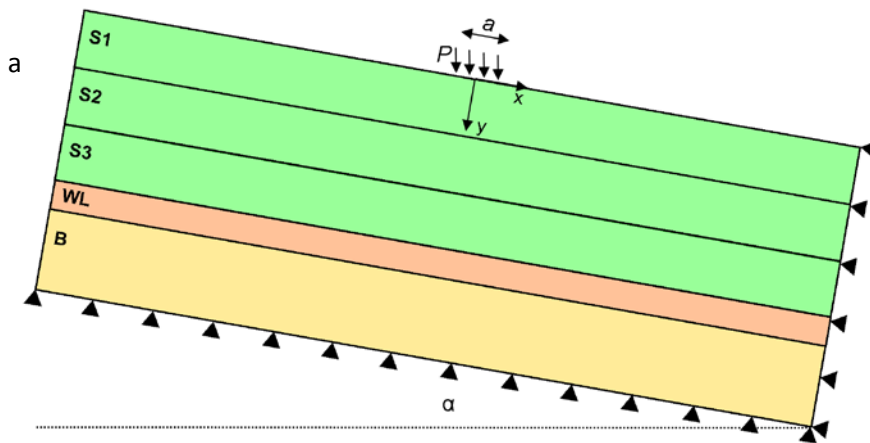


505  
 506 Figure 2: Sketch presenting the propagation saw test (PST) as it is seen looking upslope: After  
 507 isolating a column 30 cm wide and at least 1.2 m upslope, the weak layer is cut with a snow saw from  
 508 its lower end continuing upslope. Possible fracture results are described in the inset. Here, we only  
 509 consider tests where the fracture went to the end of the column (End).

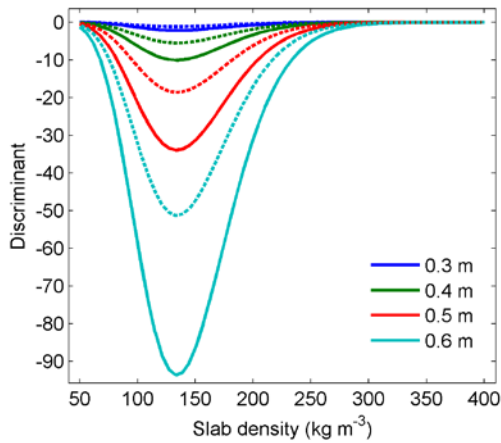




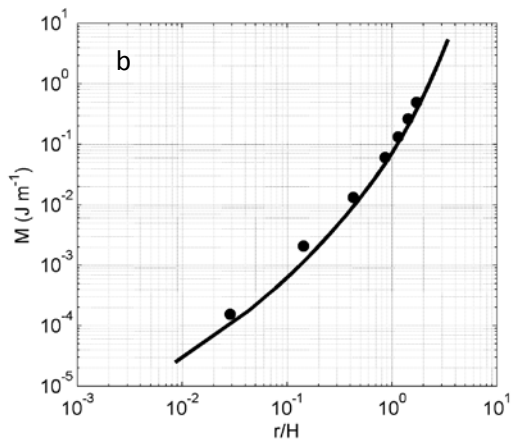
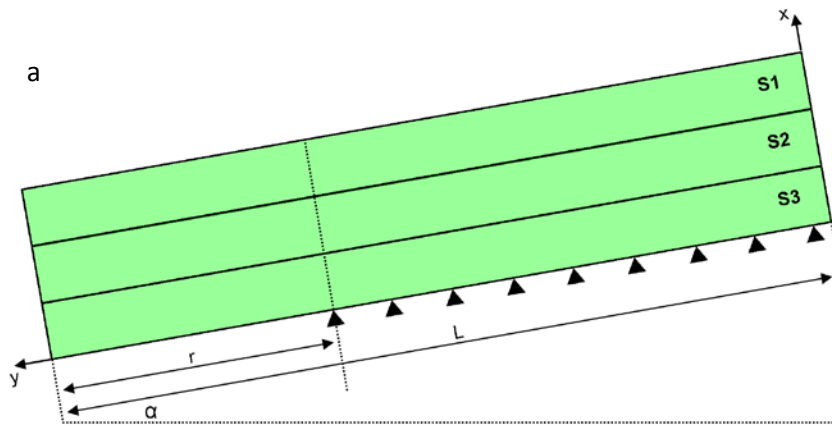
510 Figure 3: Penetration resistance (black) as measured with the SMP vs. snow depth. Slab layers (S1 to  
 511 S5) shaded in light green, weak layer (W) shaded in light red, basal layer (B) shaded in light orange.  
 512 50 mm of air signal cut off.



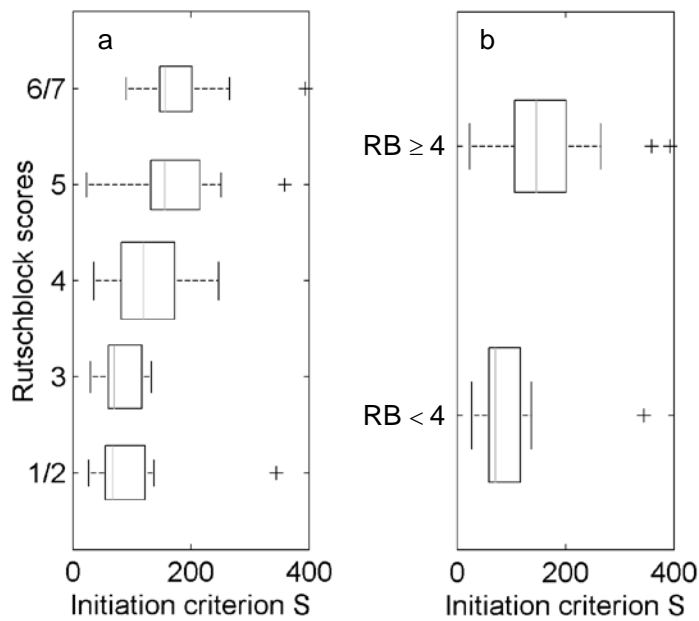
513 Figure 4: (a) FE model to simulate the maximum shear stress at the depth of the weak layer  
 514 consisting of three slab layers (green), the weak layer (red) and a basal layer below (orange) inclined  
 515 by the slope angle  $\alpha$ . Triangles indicate fixed nodes. The applied strip load  $P$  is illustrated by black  
 516 arrows pointing towards the snow surface. The axes of the coordinate system are indicated by  
 517 arrows. (b) Maximum shear stress from FE simulations (dots) and from the analytical solution (line)  
 518 for a uniform slab with density  $200 \text{ kg m}^{-3}$  and a slope angle of  $38^\circ$  versus slab thickness  $H$ .



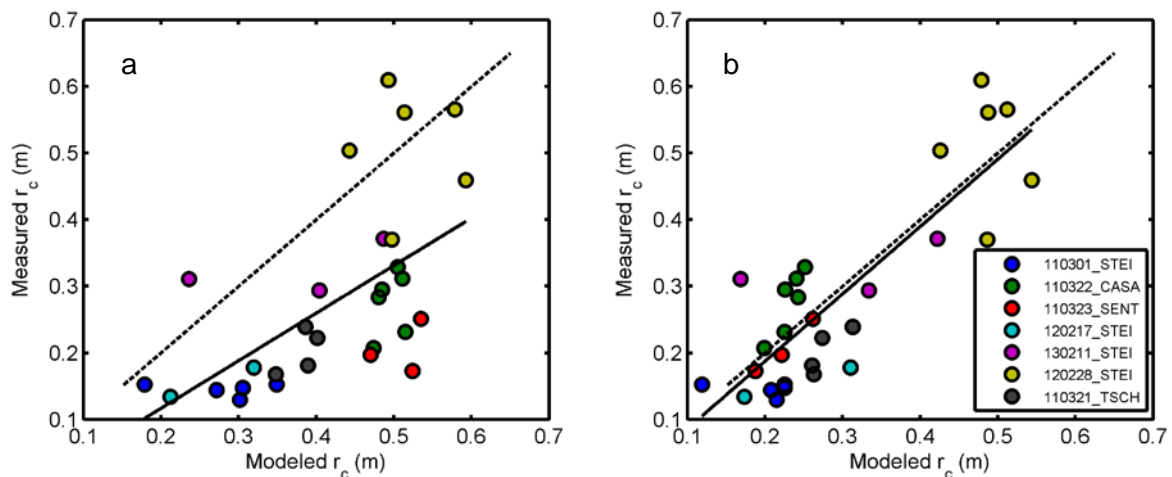
519 Figure 5: The polynomial's (Eq. 5) discriminant versus slab density for typical values of slab thickness  
 520 (colors); different line styles indicate flat terrain (dashed) and a slope inclined by  $\alpha = 38^\circ$  (solid lines).



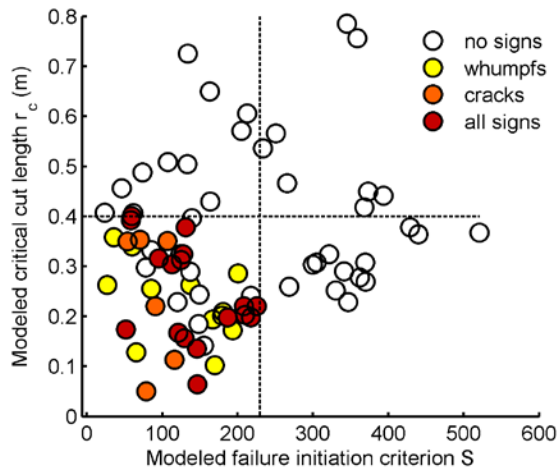
521 Figure 6: (a) The FE model to calculate the equivalent effective modulus contains as many slab layers  
 522 as necessary to reflect the stratigraphy found in the SMP signal. Triangles indicate fixed nodes. The  
 523 beam of length  $L$  is overhanging a crack of length  $r$  and is inclined by the slope angle  $\alpha$ . (b)  
 524 Mechanical energy  $M$  over the ratio of crack length and slab thickness ( $r/H$ ) modeled with FE (dots)  
 525 and calculated from the analytical solution (line) for a homogeneous slab with density  $200 \text{ kg m}^{-3}$  and  
 526 a slope angle of  $30^\circ$ .



527 Figure 7: Modeled failure initiation criterion  $S$  (a) vs. RB score and (b) vs. RB stability classes: RB < 4  
 528 (N = 38) and RB  $\geq$  4 (N = 26). Boxes span the interquartile range from 1st to 3rd quartile with a  
 529 horizontal line showing the median (grey line). Widths of the boxes correspond to the number of  
 530 cases. Whiskers extend to the most extreme data points not considered outliers (crosses) within 1.5  
 531 times the interquartile range above the 3<sup>rd</sup> and below the 1<sup>st</sup> quartile.



532 Figure 8: Critical crack lengths  $r_c$  predicted from Eq. 7 are contrasted with critical crack lengths  
 533 measured in the field (N = 31). Experiments grouped by date and location with colors. Solid line  
 534 shows linear regression, dashed line indicates the 1:1 line. (a) Slab stratigraphy neglected (average  
 535 density, average effective modulus). (b) Density and effective modulus of each snow layer taken into  
 536 account by FE simulation.



537 Figure 9: Type and presence of signs of instability against failure initiation criterion  $S$  and critical crack  
 538 length  $r_c$ , both modeled, for datasets A and B, if reported ( $N = 77$ ). Colors indicate type of observed  
 539 signs of instability: whumpfs, shooting cracks with or without whumpfs (cracks) or all signs  
 540 (whumpfs, cracks and recent avalanches observed). Open circles indicate that no signs of instability  
 541 were reported explicitly (no signs). Dashed lines represent split values dividing the plot into four  
 542 quadrants as found with a classification tree.